SUPPORTING INFORMATION

$[(Cp_2M)_2B_9H_{11}]$ (M = Zr or Hf): early transition metal 'guarded' heptaborane with strong covalent and electrostatic bonding

Anangsha De,[a] Qian-Fan Zhang,[‡b] Bijan Mondal,[‡a] Ling Fung Cheung,[b] Sourav Kar,[a] Koushik Saha,[a] Babu Varghese,[c] Lai-Sheng Wang,*[b] and Sundargopal Ghosh*[a]

[a]*Department of Chemistry, Indian Institute of Technology Madras, Chennai 600036, India*
[b]*Department of Chemistry, Brown University, Providence, Rhode Island 02912, United States*
[c]*Sophisticated Analytical Instruments Facility, Indian Institute of Technology Madras, Chennai 600036, India*

Table of Contents

I Synthesis and characterizations

General procedures and instrumentation: All manipulations were carried out under argon atmosphere using Schlenk line or glovebox techniques. Solvents (toluene, dichloromethane, hexane etc.) were dried by common methods and distilled under Ar prior to use. $[Cp_2ZrCl_2]$, $[Cp_2HfCl_2]$, $LiBH_4$ 2.0 M in THF and $[BH_3.THF]$ were purchased from Sigma Aldrich and used as received. The external reference, $[Bu_4N][B_3H_8]$, for the ^{11}B NMR was synthesized following the literature method.[1] Thin layer chromatography was carried on 250 mm diameter aluminum supported silica gel TLC plates (MERCK TLC Plates). NMR spectra were recorded on a 500 MHz Bruker FT-NMR spectrometer. Residual solvent protons were used as reference (δ, ppm, $CDCl_3$, 7.26; [*d*$_6$]-benzene = 7.16), while a sealed tube containing $[Bu_4N][B_3H_8]$ in [*d*$_6$]-benzene (δ_B, ppm, –30.07) was used as an external reference for the ^{11}B NMR. Mass spectra were recorded on Micromass Q-TOF Micro instrument. Flow injection analysis of samples were performed on an Agilent 6530 Accurate Mass Q-TOF mass spectrometer coupled to Agilent 1260 LC system. The ESI mobile phase was introduced at a flow rate of 200 μL/min. Agilent 6530 QTOF was operated in extended dynamic range using the following dual ESI source settings; drying gas: 8 L/min, gas temperature: 130°C, nebulizer: 35 psig, capillary voltage: 3500 V, fragmentor: 60 V, skimmer: 65 V. The full-scanned MS and collision-induced dissociation (MS/MS) spectra were recorded at a rate of 1 spectrum/s. Targeted MS/MS spectra were obtained at selected collision energies, and precursor parent ion was isolated with an *m/z* width of ~ 4. Data were processed using Agilent MassHunter qualitative analysis software (version B.06).

Synthesis of [$(Cp_2Zr)_2B_9H_{11}$] (1) and [$(Cp_2Zr)_2B_5H_{11}$] (I). To the solution of in situ generated [$Cp_2Zr(BH_4)_2$] in toluene, an excess amount of [BH_3.THF] was added and refluxed at 100 °C for 24h. After removing the solvent under vacuum, the residue was extracted through celite using hexane/dichloromethane mixture. The filtrate was concentrated and the residue was subjected to chromatographic workup on silica gel TLC plates. Elution with a hexane/dichloromethane (20:80 v/v) mixture yielded colourless **1** (0.035g, 15%) along with **I** (0.054g, 35%). Isolated yields are calculated based on the amount of Cp_2ZrCl_2 (0.5g) used.

1: $^{11}B\{^1H\}$ NMR (22 °C, 160 MHz, $CDCl_3$): δ 29.1 (br 1B), 21.6 (br, 1B), 16.9 (br, 1B), 13.2 (br, 1B), 6.8 (br, 1B). 6.3 (br, 1B), 0.8 (br, 1B), -3.6 (br, 2B). ^1H NMR (22 °C, 500 MHz, $CDCl_3$): δ 6.13 (s, 10H, 2Cp), 6.06 (s, 10H, 2Cp), -1.40 (br). $^1H\{^{11}B\}$ NMR (22 °C, 500 MHz, $CDCl_3$): δ 6.13 (s, 10H, 2Cp), 6.06 (s, 10H, 2Cp), 3.31 (s, 1H, B-H_t), 0.50 (s, 2H, B-H_t, B-H_t), -1.10 (s, 1H, Zr-H-B), -1.70 (s, 1H, Zr-H-B). $^{13}C\{^1H\}$ NMR (22 °C, 125 MHz, C_6D_6): δ 109.7, 109.1 (C_5H_5). IR (dichloromethane, cm^{-1}): $\bar{\upsilon}$ = 2529, 2481 (B-H_t).

Synthesis of and [$(Cp_2Hf)_2B_9H_{11}$] (2) and [$(Cp_2Hf)_2B_5H_{11}$] (II). To the solution of in situ generated [$Cp_2Hf(BH_4)_2$] in toluene, an excess amount of [BH_3.THF] was added and refluxed at 110 °C for 24h. The reaction mixture was filtered through celite. The filtrate was concentrated, and the residue was chromatographed on silica gel TLC plates. Elution with a hexane/dichloromethane (20:80 v/v) mixture yielded colourless **2** (0.024 g, 10%) along with pale yellow **II** (0.063g, 28%). Isolated yields are calculated based on the amount of [Cp_2HfCl_2] (0.5g) used.

2: $^{11}B\{^1H\}$ NMR (22 °C, 160 MHz, C_6D_6): δ 28.7 (br 1B), 21.5 (br, 1B), 17.8 (br, 1B), 16.2 (br, 1B), 6.5 (br, 1B), 5.0 (br, 1B), 2.4 (br, 1B), -3.4 (br, 2B). ^1H NMR (22 °C, 500 MHz, C_6D_6): δ 5.57 (s, 10H, 2Cp), 5.51 (s, 10H, 2Cp), -0.42 (br), -0.82 (br), -1.23 (br). $^1H\{^{11}B\}$ NMR (22 °C, 500 MHz, $CDCl_3$): δ 6.03 (s, 10H, 2Cp), 5.97 (s, 10H, 2Cp), 3.32 (s, 1H, B(4)-H_t), 0.41 (s, 2H, B(3)-H_t, B(6)-H_t), -0.59 (s, 1H, Hf(1)-H-B(2)), -1.36 (s, 1H, Hf(2)-H-B(7)). ^1H NMR (–50 °C, 500 MHz, [d_8]-toluene): -0.64 (s, 1H, Hf(1)-H-B(2)), -1.14 (s, 1H, Hf(2)-H-B(7)), -3.26 (br, 3H, Hf-BH_3), -3.42 (br, 3H, Hf-BH_3). $^{13}C\{^1H\}$ NMR (22 °C, 125 MHz, C_6D_6): δ 108.3, 107.8 (C_5H_5). IR (dichloromethane, cm^{-1}): $\bar{\upsilon}$ = 2540, 2486 (B-H_t).

II: MS (ESI^+, [M^+]): calculated mass for $C_{20}H_{31}B_5Hf_2$: 686.2, obsd: 686.4. $^{11}B\{^1H\}$ NMR (22 °C,160 MHz, $CDCl_3$): δ 4.6 (br 2B), 2.0 (br, 1B), -3.8 (br, 2B). ^1H NMR (22 °C, 500 MHz, $CDCl_3$): δ 5.92 (s, 10H, 2Cp), 5.90 (s, 5H, 1Cp), 5.89 (s, 5H, 1Cp), -2.74 (br, 1H, B-H-B), -4.16 (br, 4H, Hf-H-B). $^{13}C\{^1H\}$ NMR (22 °C, 125 MHz, $CDCl_3$): δ 107.5, 106.5 (C_5H_5). IR (dichloromethane, cm^{-1}): $\bar{\upsilon}$ = 2494, 2423 (B-H_t).

II Mass spectrometry details

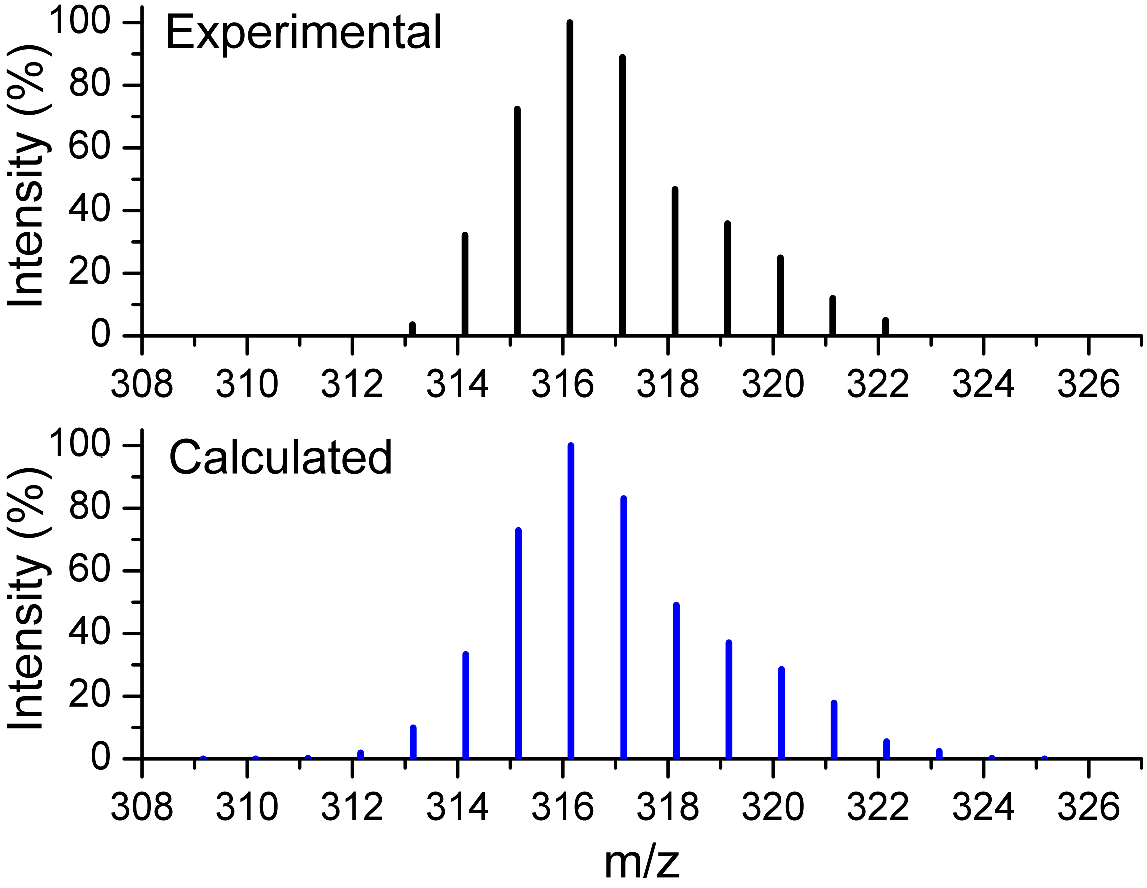

Fig. S1. The mass spectrum (ESI negative mode) of compound **1** in 100% MeCN (top); calculated isotopic distribution of $[M-(Cp_2Zr)-BH_2]^-$ is shown at the bottom.

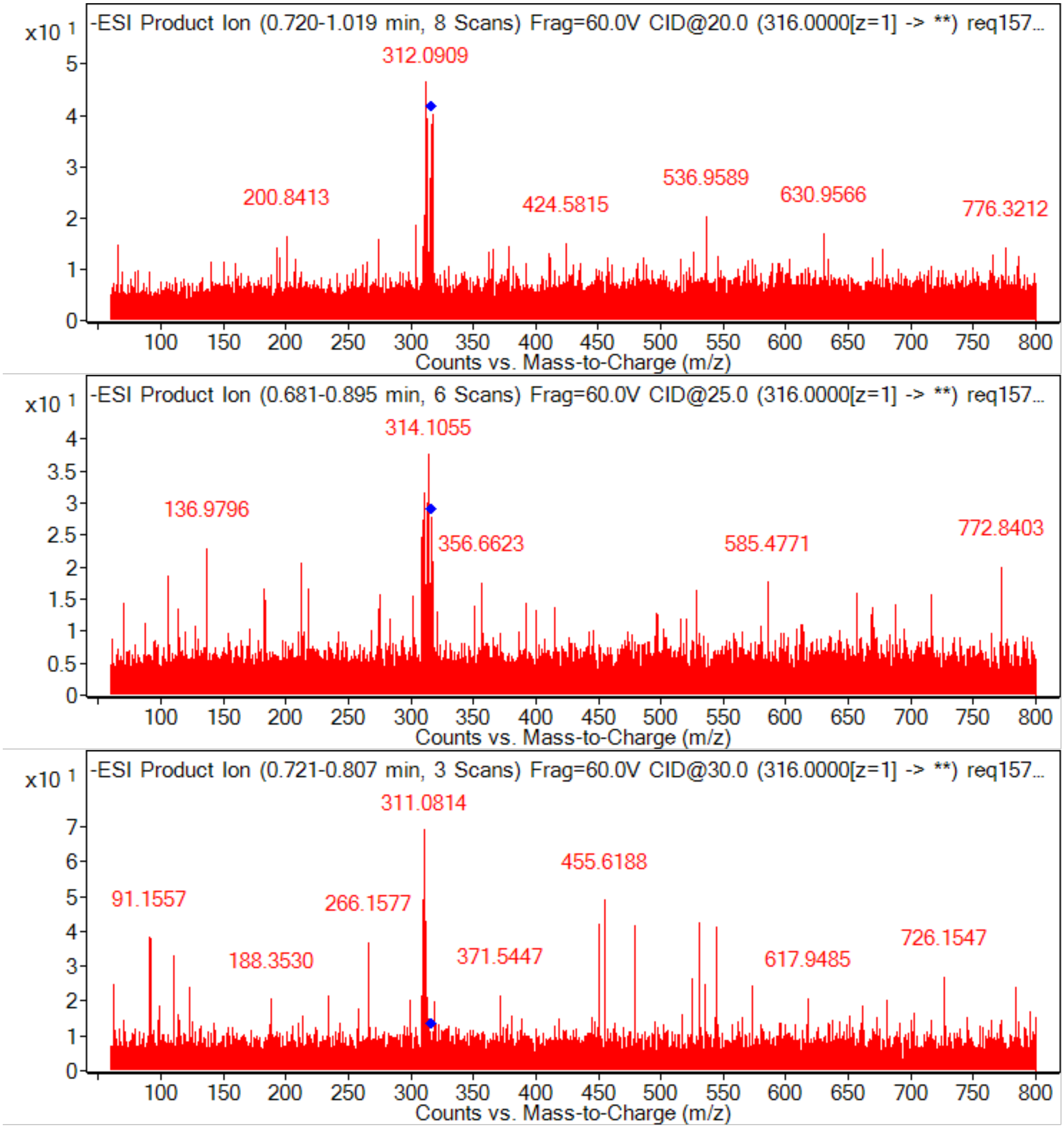

Fig. S2. The MS/MS (ESI negative mode) of compound **1** in 100% MeCN; collision energies are 20 V, 25 V, 30 V from top to bottom. The blue squares indicate the positions of the parent ion.

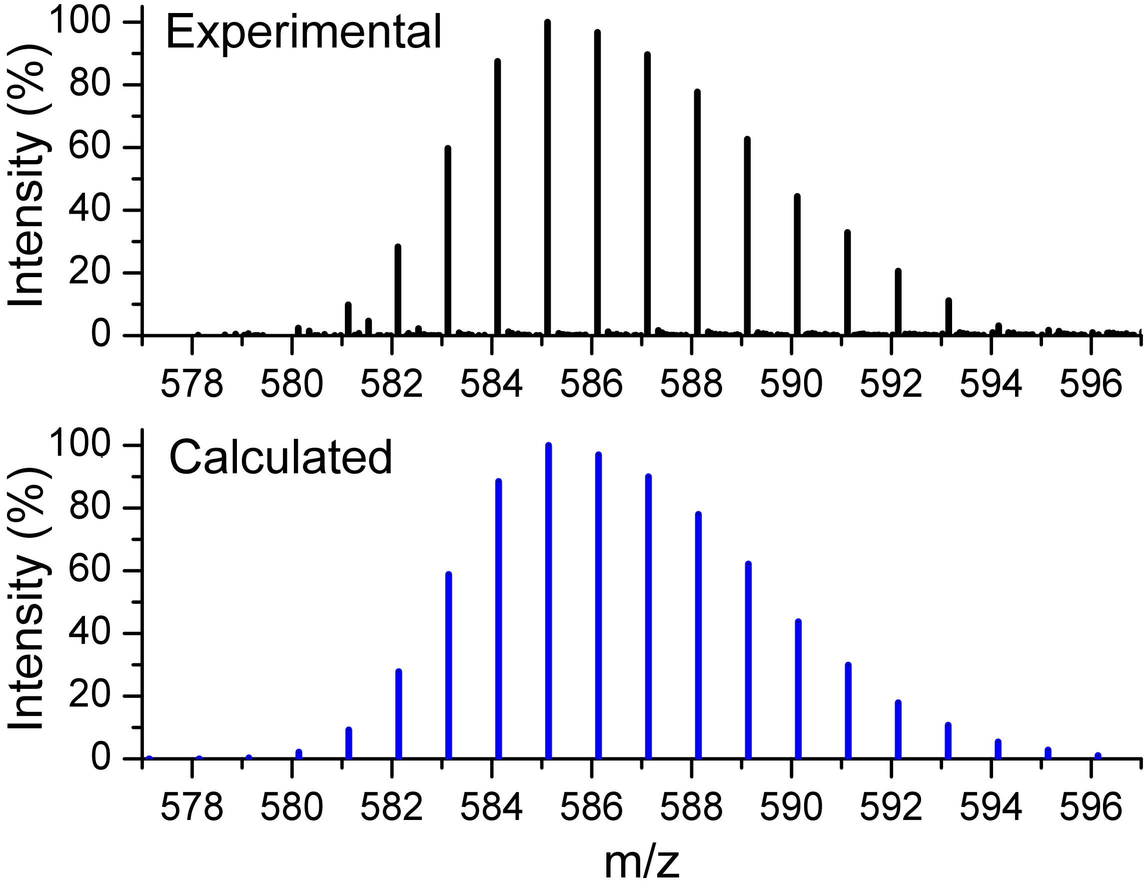

Fig. S3. The mass spectrum (ESI negative mode) of compound **1** in 95% MeCN + 5% H_2O (top); calculated isotopic distribution of $[M+Cl]^-$ is shown at the bottom.

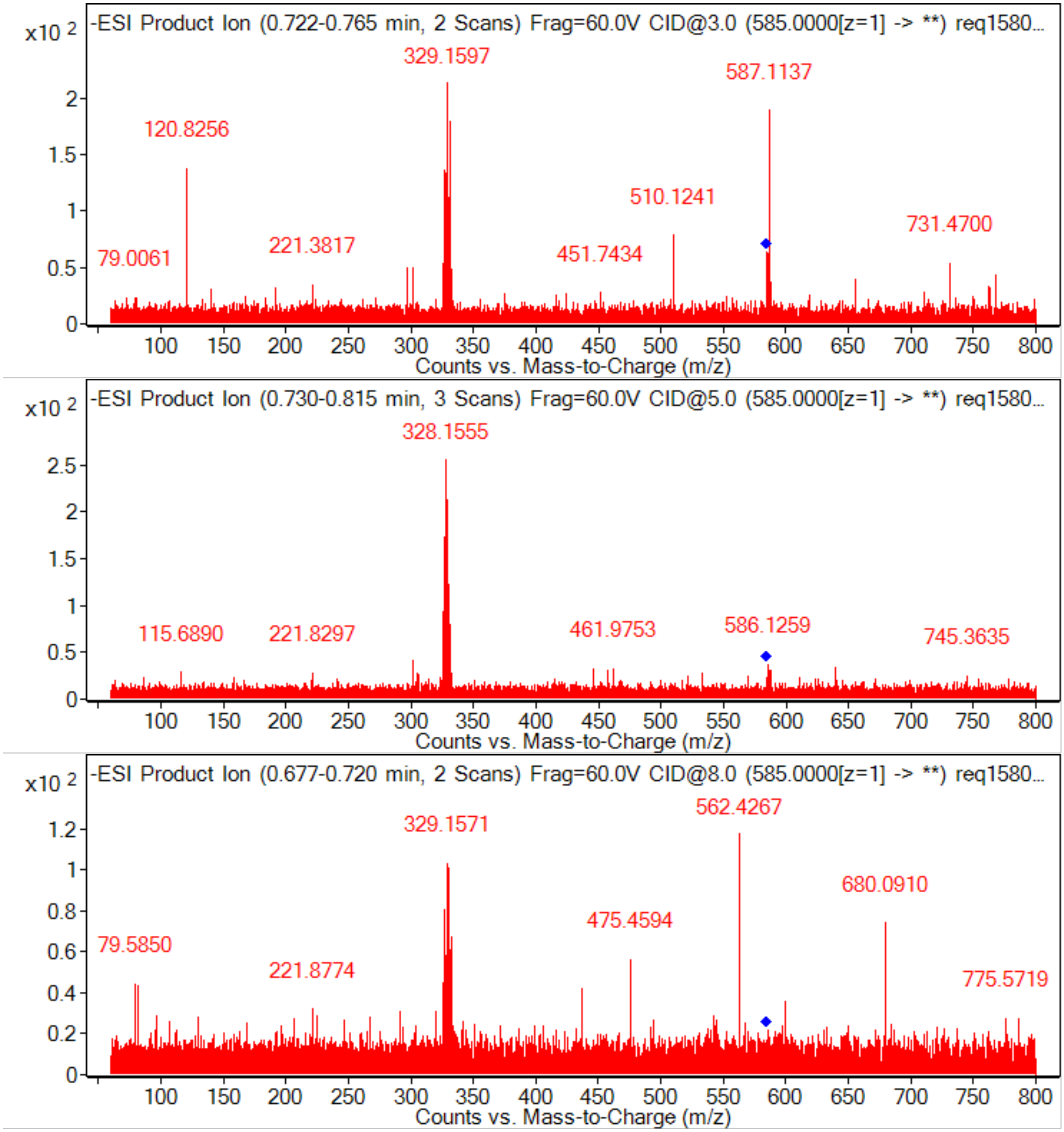

Fig. S4. The MS/MS (ESI negative mode) of compound **1** in 95% MeCN – 5% H_2O; collision energies are 3 V, 5 V, 8 V from top to bottom. The blue squares indicate the positions of the parent ion. The most abundant isotope of $[M\text{-}(Cp_2Zr)]^-$ has calculated m/z = 329.18512.

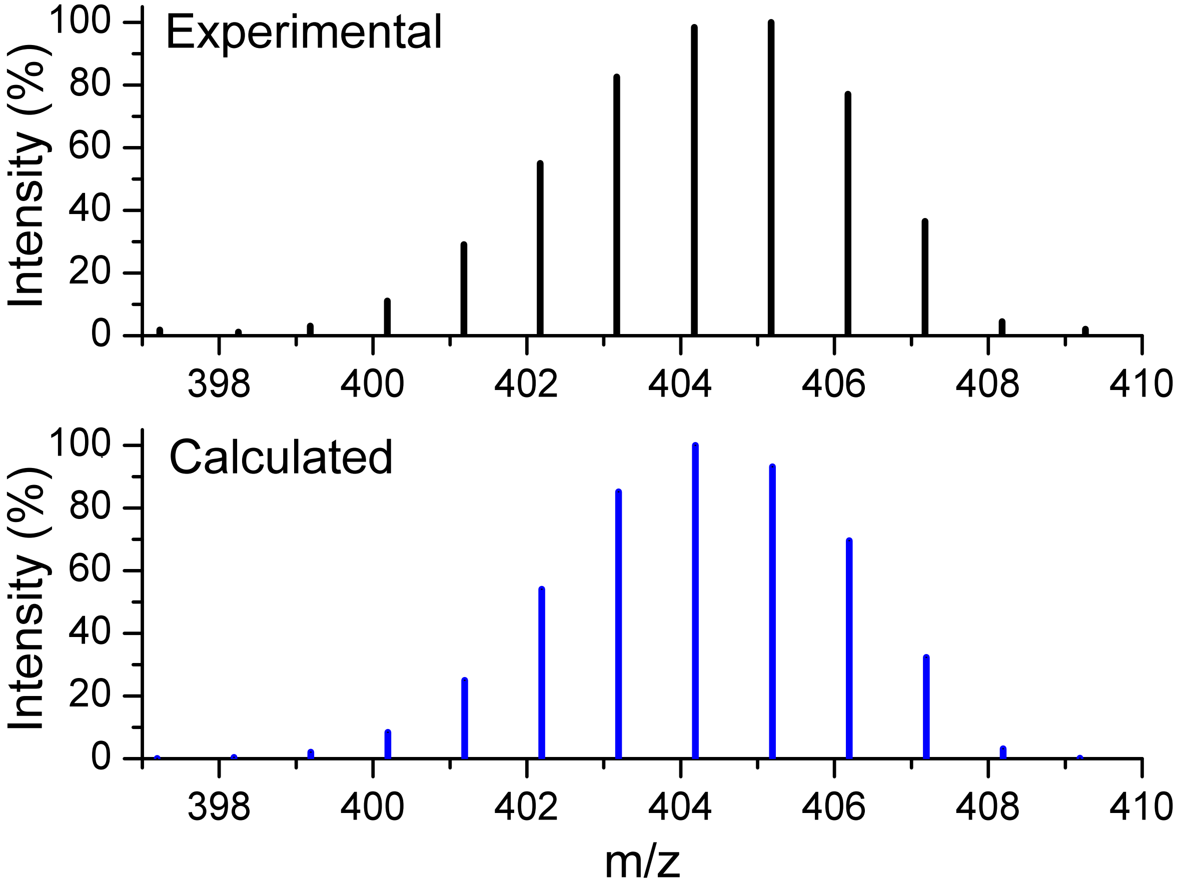

Fig. S5. The mass spectrum (ESI negative mode) of compound **2** in 100% MeCN; calculated isotopic distribution of [M-(Cp_2Hf)-BH_2]$^-$ is shown at the bottom.

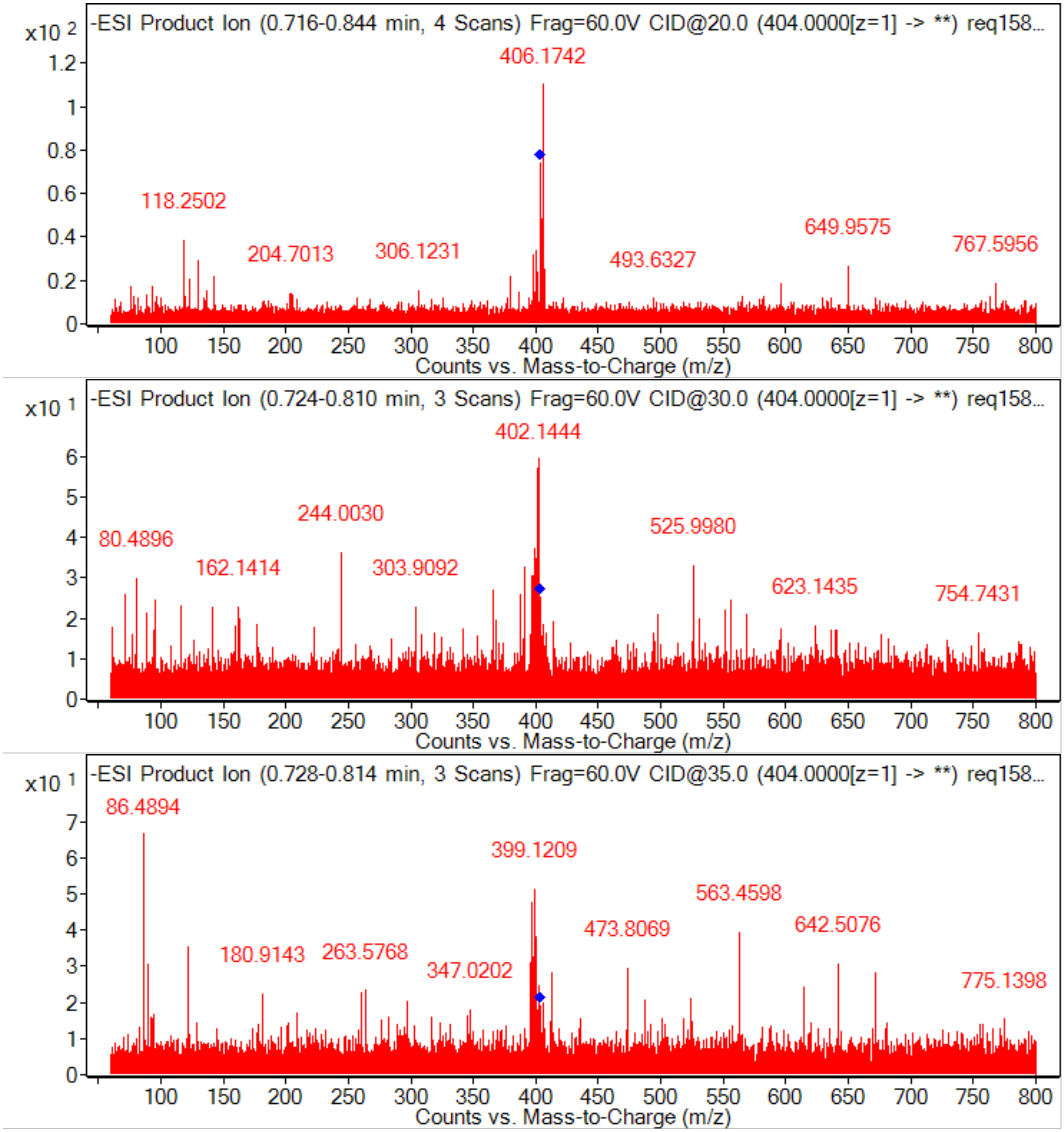

Fig. S6. The MS/MS (ESI negative mode) of compound **2** in 100% MeCN; collision energies are 25 V, 30 V, 35 V from top to bottom. The blue squares indicate the positions of the parent ion.

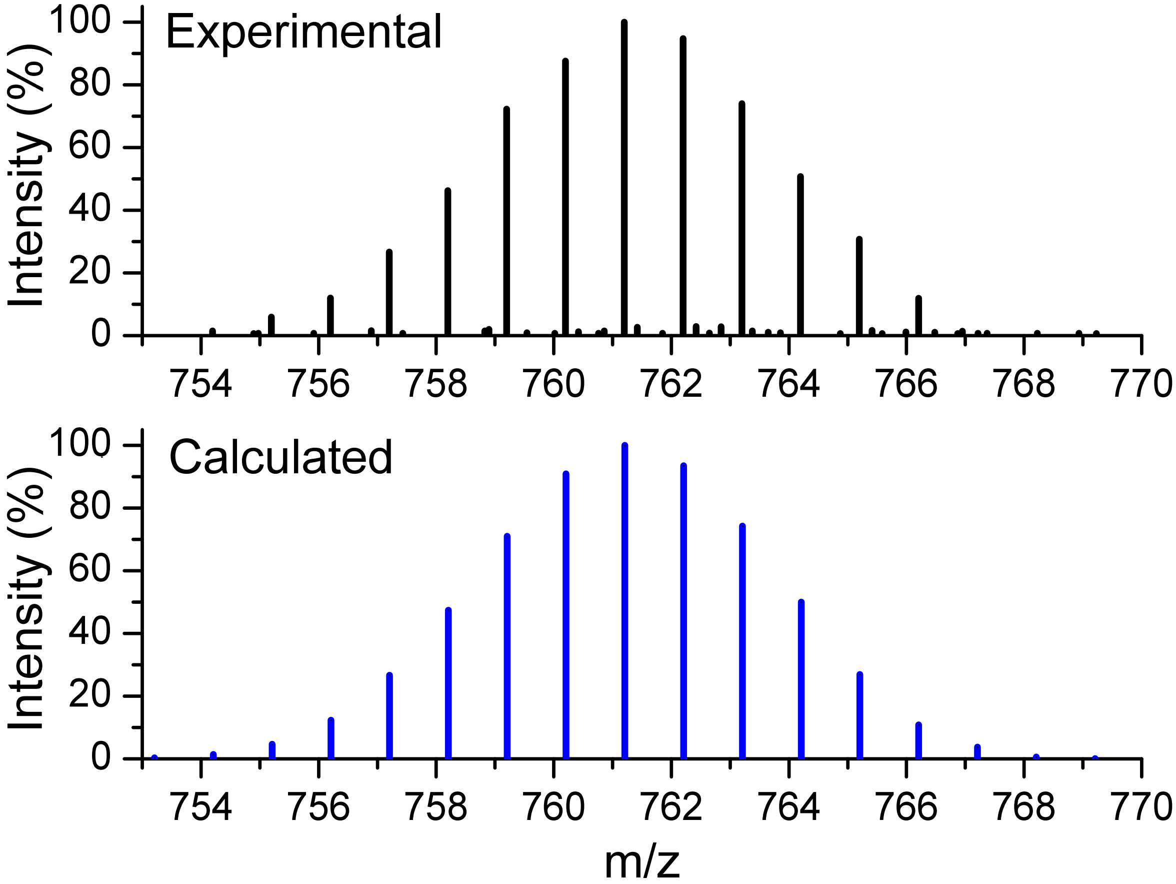

Fig. S7. The mass spectrum (ESI negative mode) of compound **2** in 95% MeCN + 5% H_2O (top); calculated isotopic distribution of $[M+Cl]^-$ is shown at the bottom.

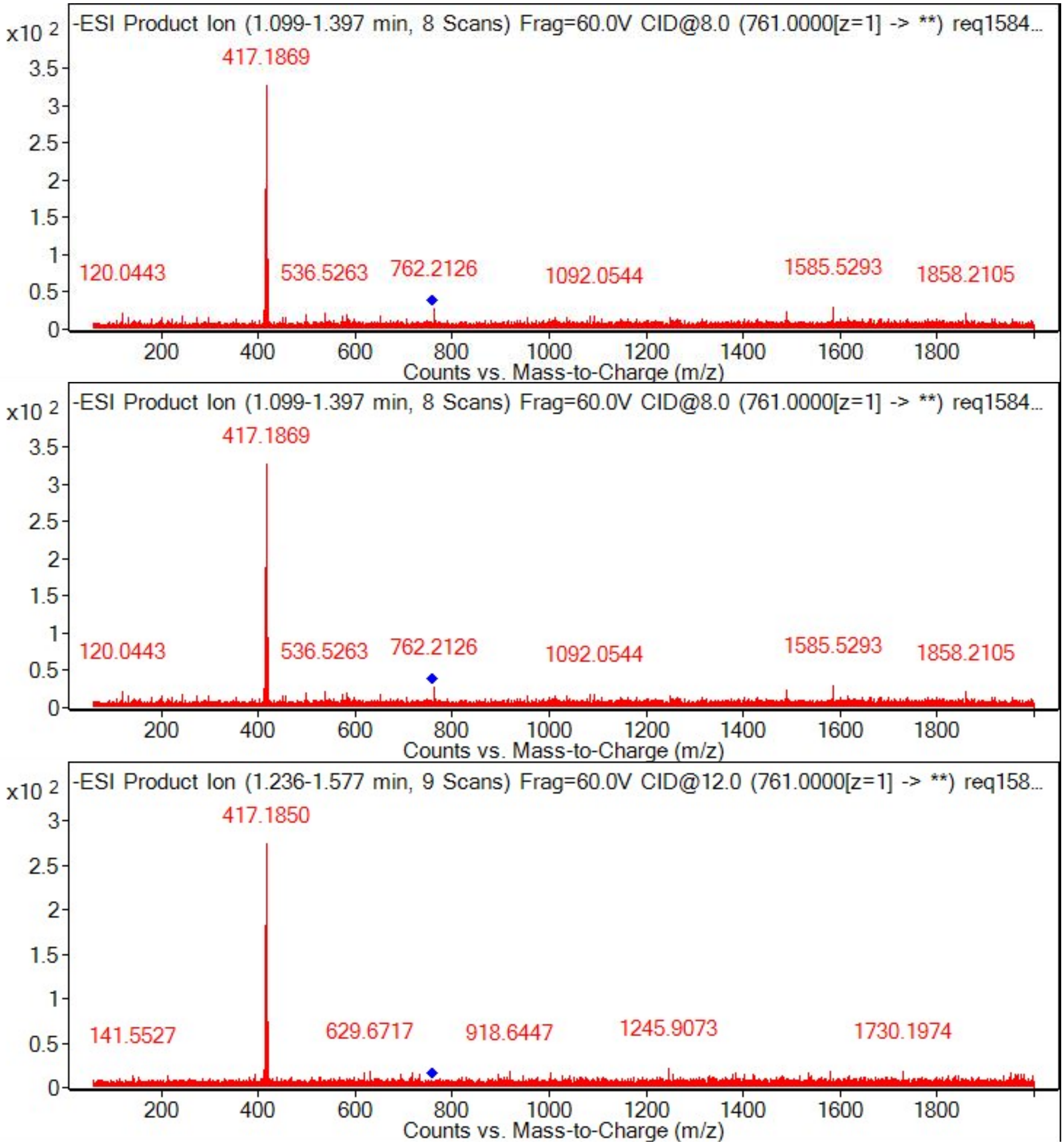

Fig. S8. The MS/MS (ESI negative mode) of compound **2** in 95% MeCN – 5% H_2O; collision energies are 5 V, 8 V, 12 V from top to bottom.

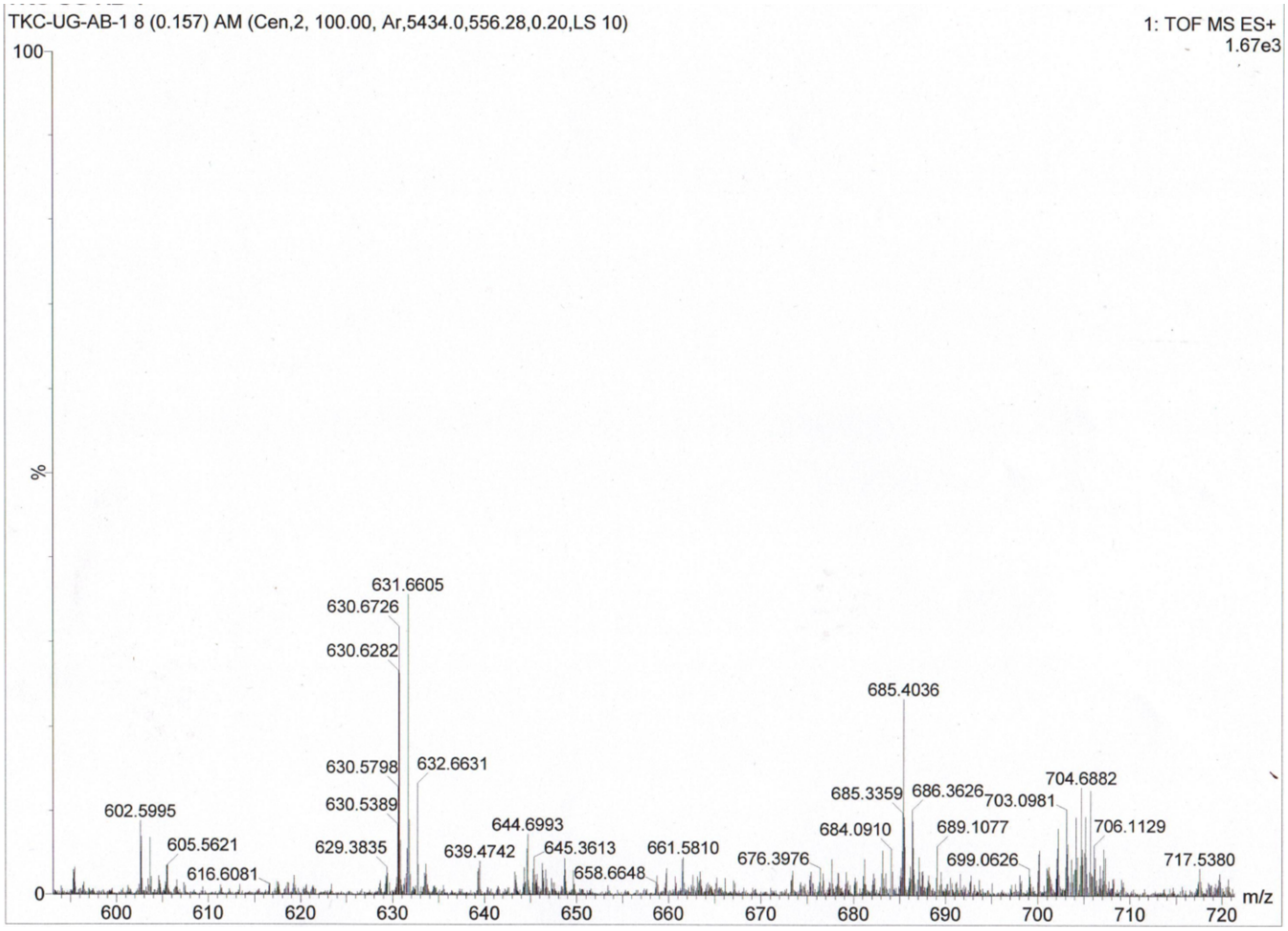

Fig. S9. ESI MS spectrum of compound **II**.

III NMR and IR spectra details

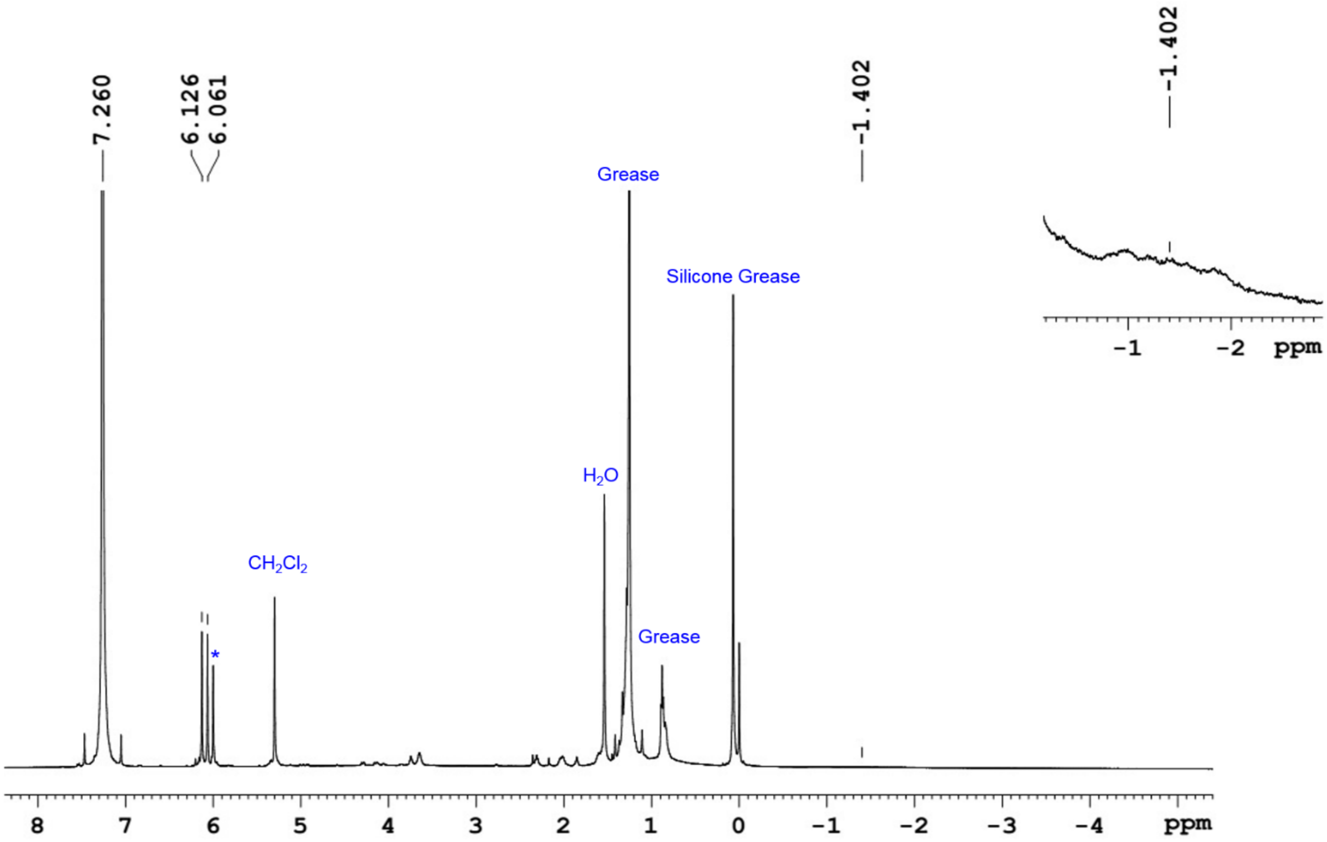

Fig. S10. ^{1}H NMR spectrum of **1** in CDCl$_3$. (* ^{1}H chemical shift at $\delta = 5.94$ ppm corresponding to inseparable impurity)

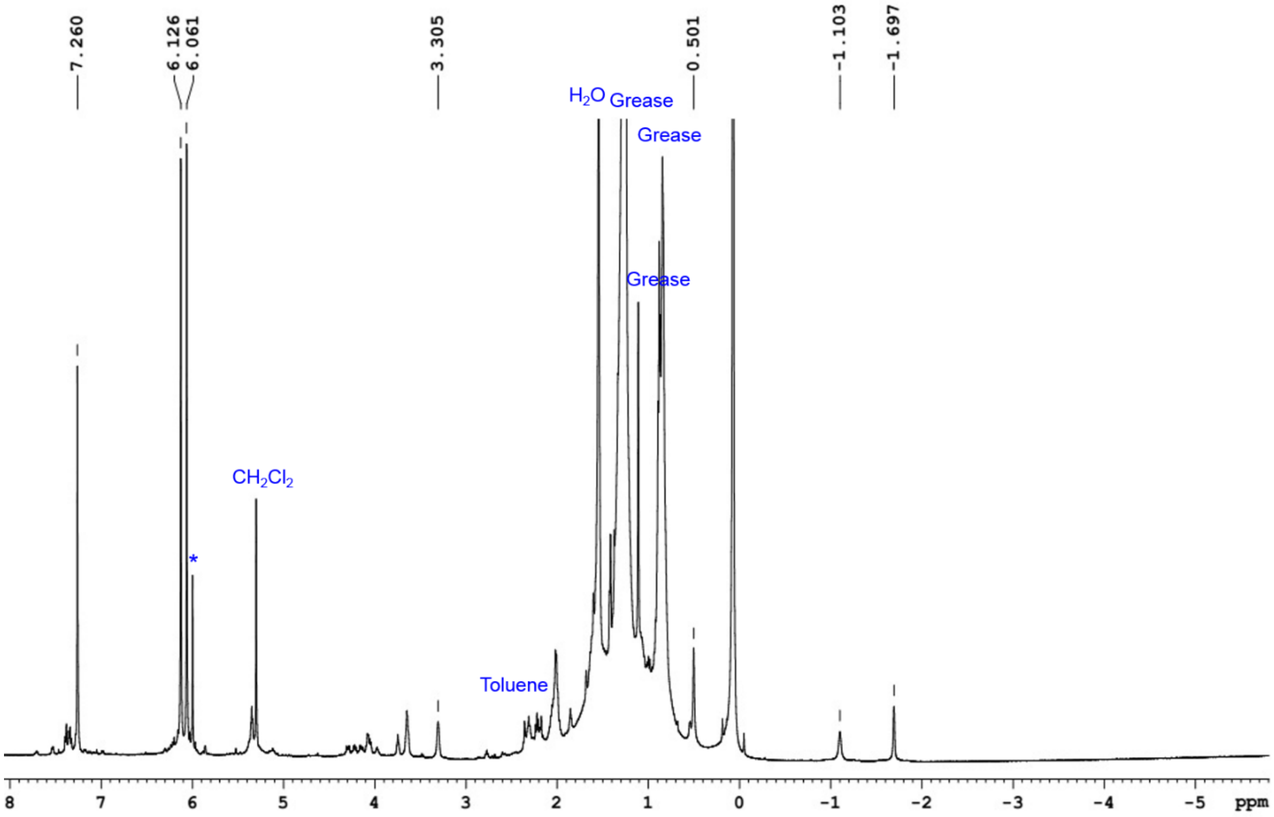

Fig. S11. $^{1}H\{^{11}B\}$ NMR spectrum of **1** in $CDCl_3$. (* ^{1}H chemical shift at δ = 5.94 ppm corresponding to inseparable impurity)

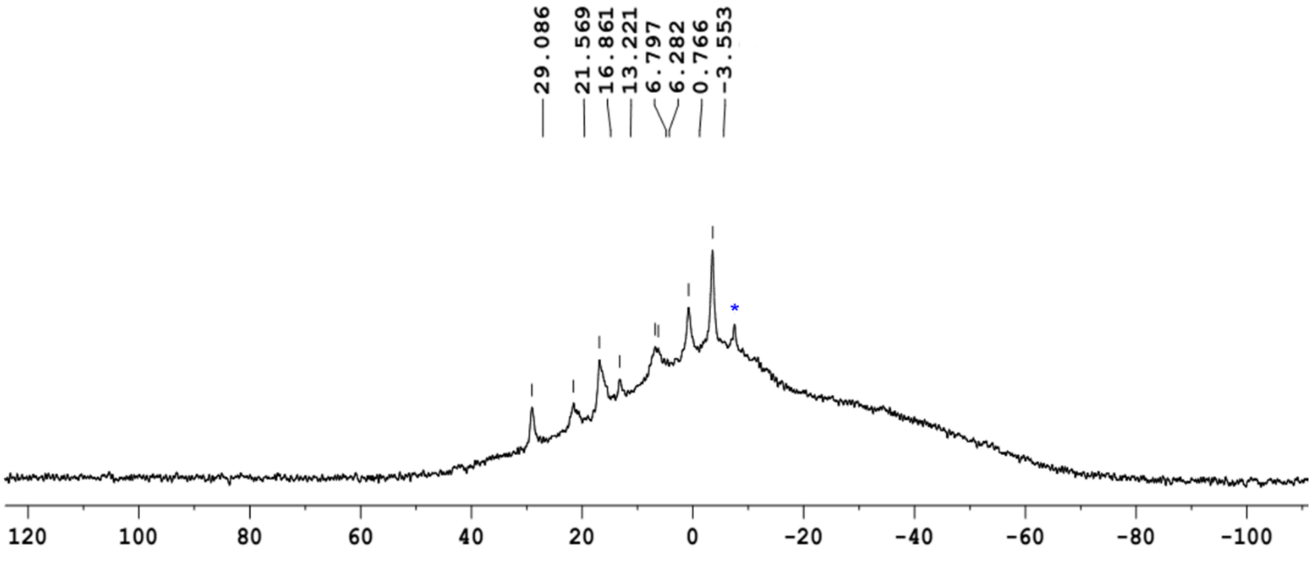

Fig. S12. $^{11}B\{^{1}H\}$ NMR spectrum of **1** in $CDCl_3$ (* ^{11}B chemical shift at δ = -7.8 ppm corresponding to inseparable impurity)

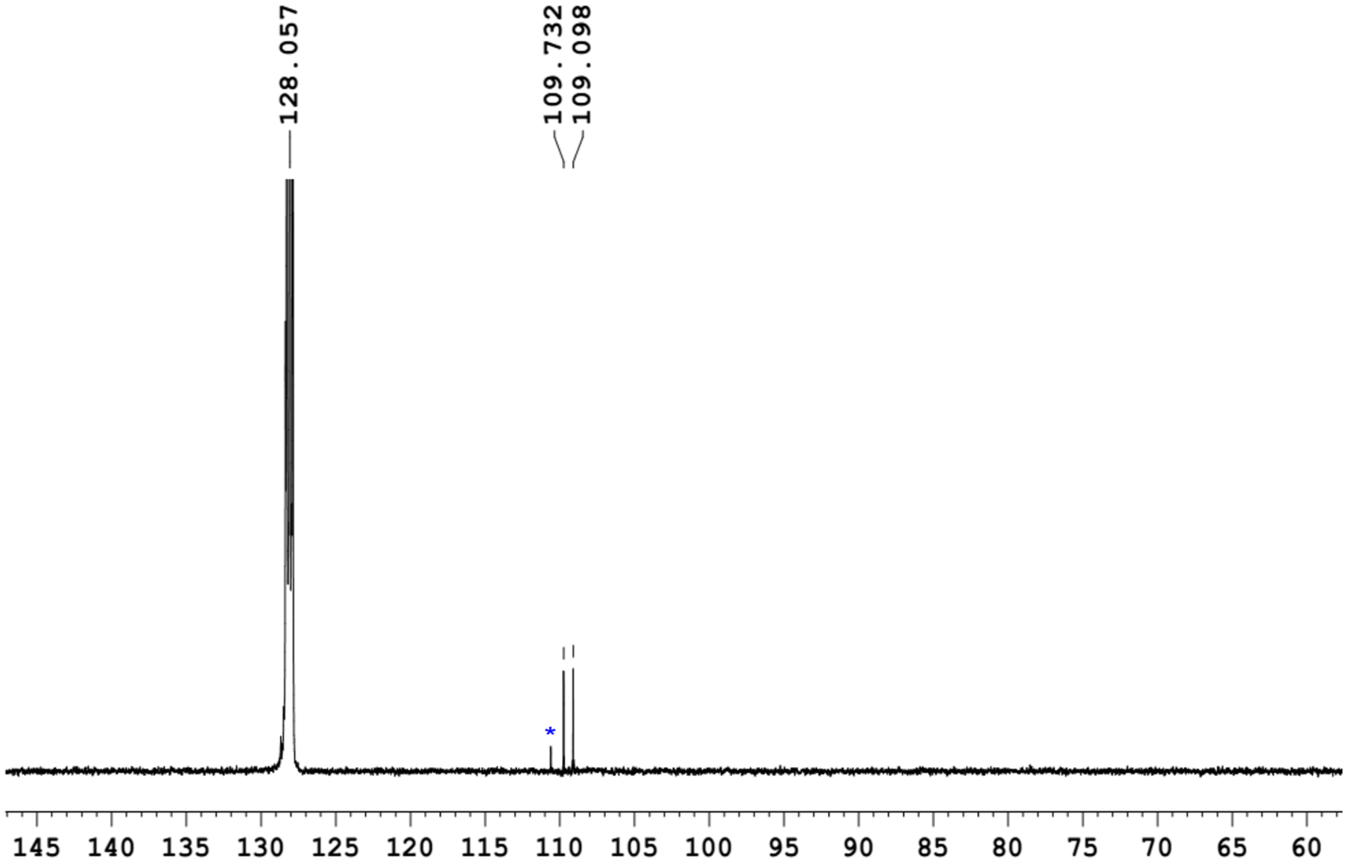

Fig. S13. $^{13}C\{^{1}H\}$ NMR spectrum of **1** in C_6D_6. (* ^{13}C chemical shift at δ = 100.8 ppm corresponding to inseparable impurity)

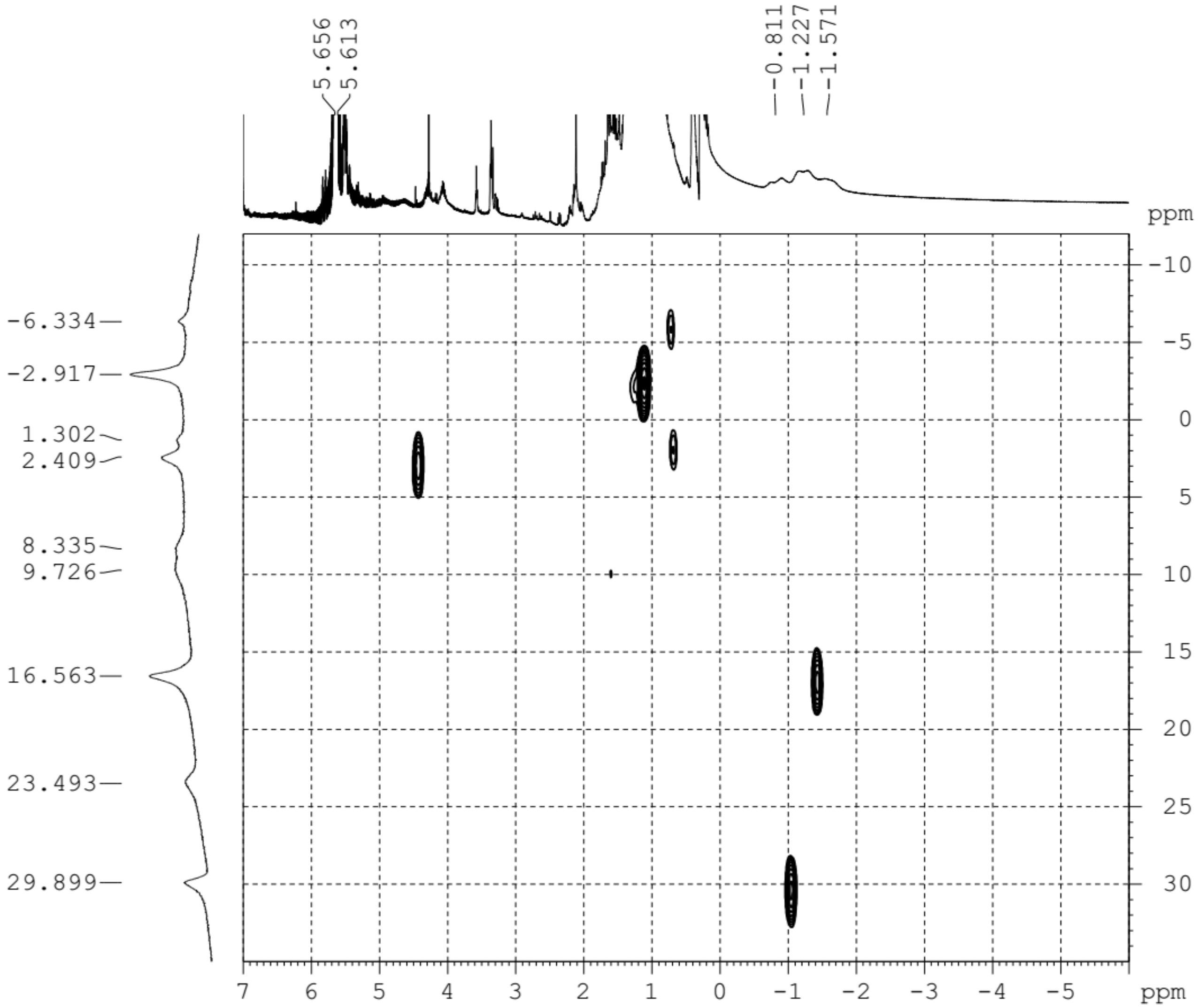

Fig. S14. $^1H/^{11}B\{^1H\}$ HSQC spectrum of **1** in C_6D_6.

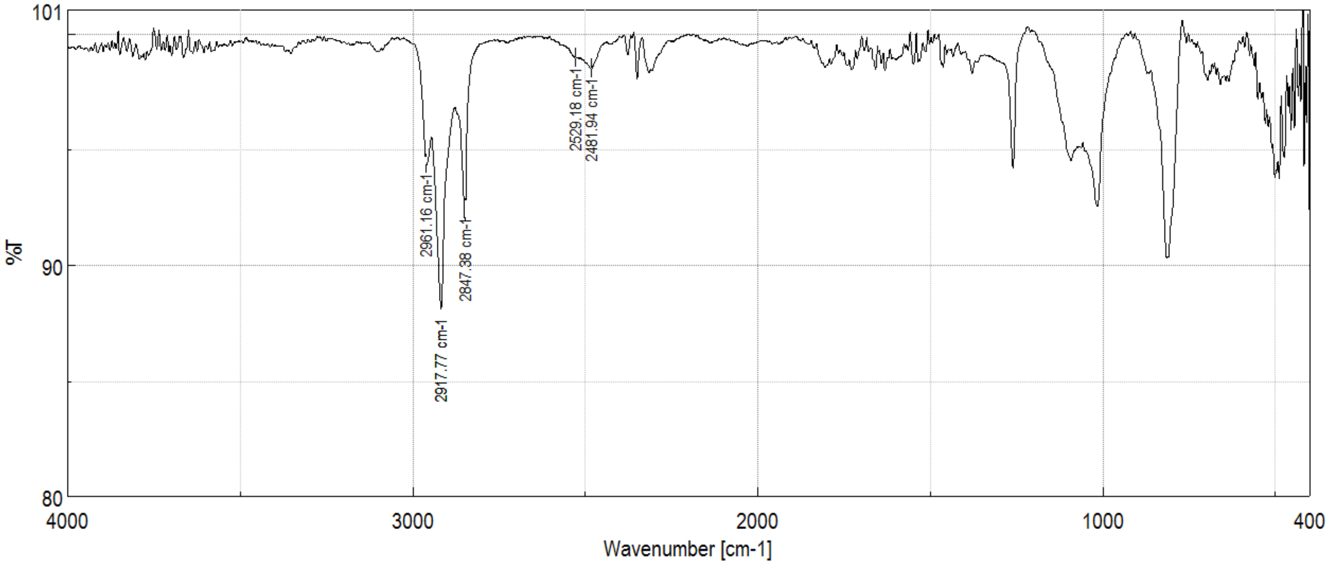

Fig. S15. IR spectrum of **1** in CH_2Cl_2.

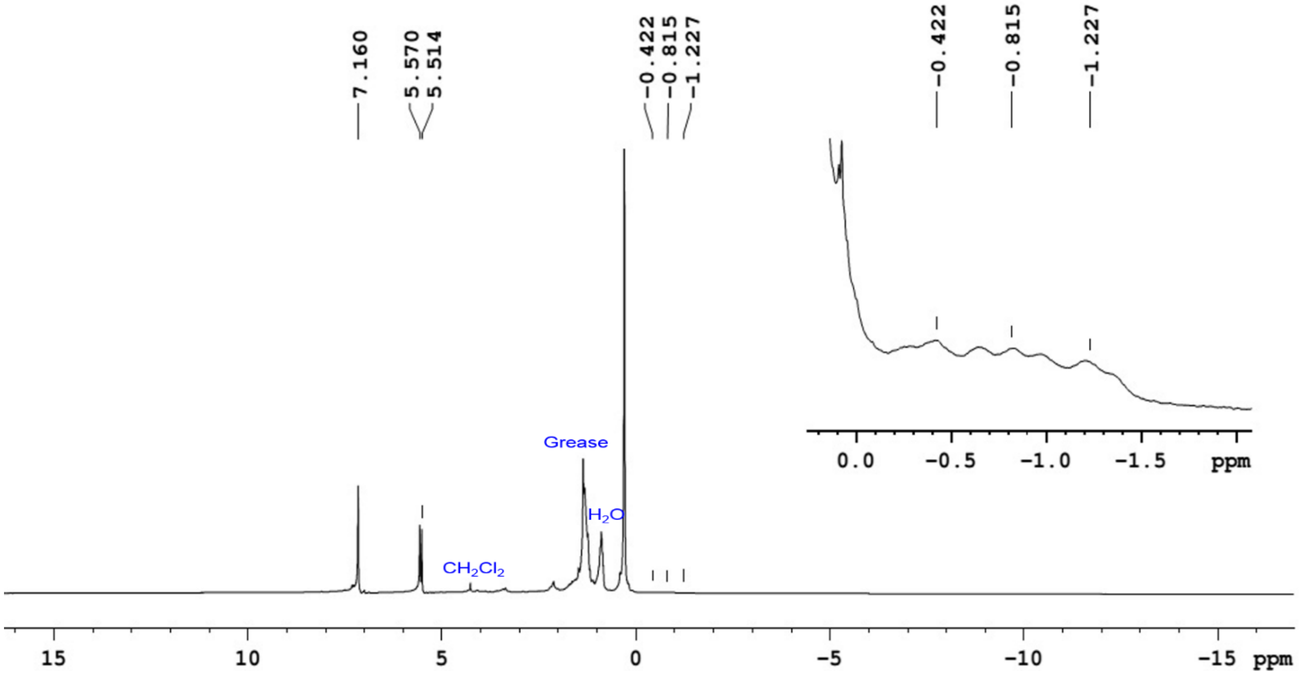

Fig. S16. ^{1}H NMR spectrum of **2** in C_6D_6.

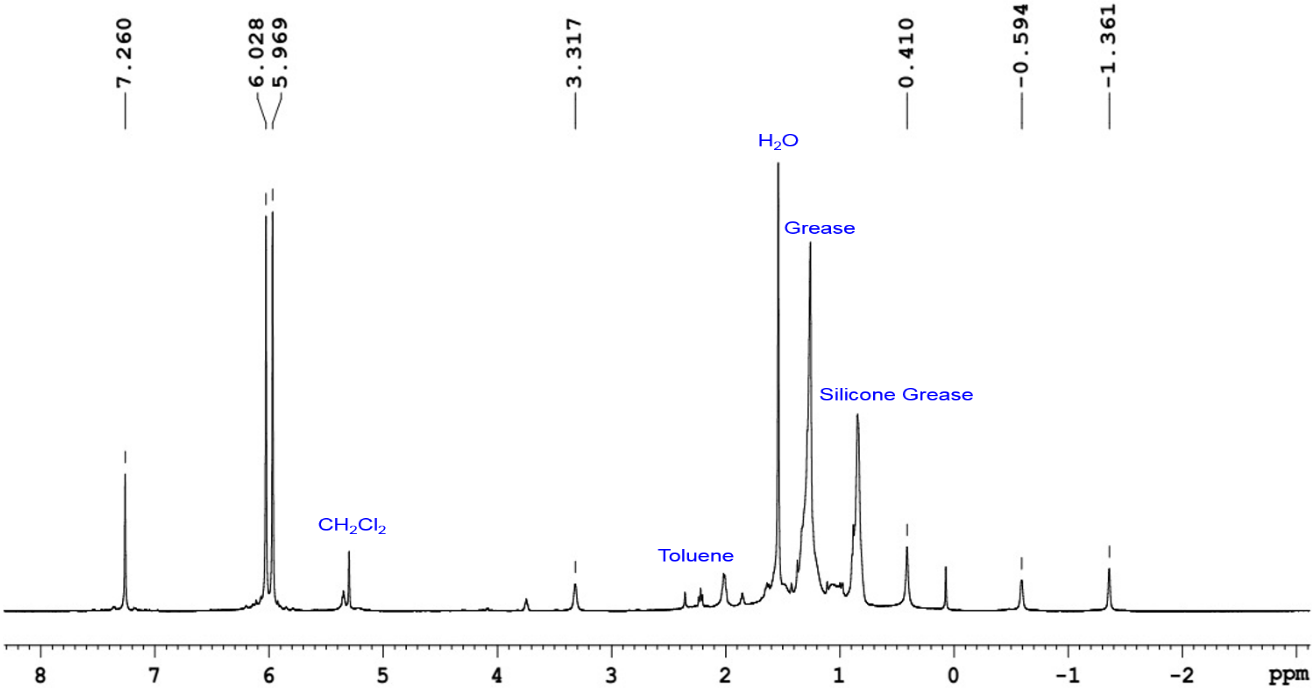

Fig. S17. ^{1}H{^{11}B} NMR spectrum of **2** in CDCl$_3$.

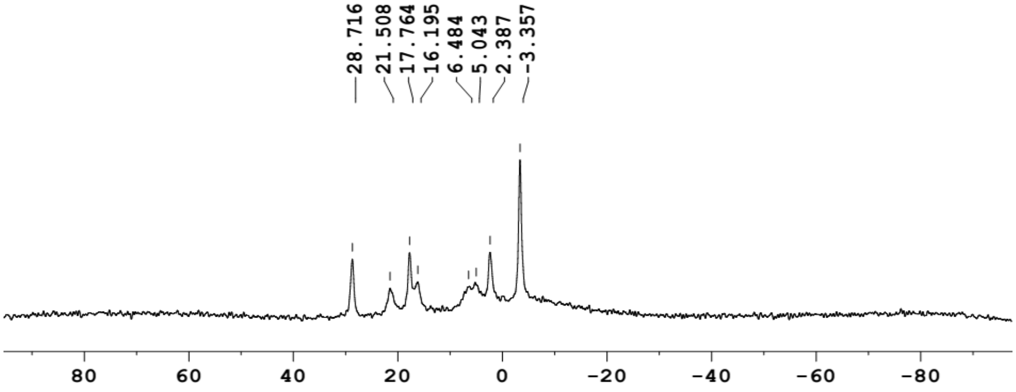

Fig. S18. ^{11}B{^{1}H} NMR spectrum of **2** in C$_6$D$_6$.

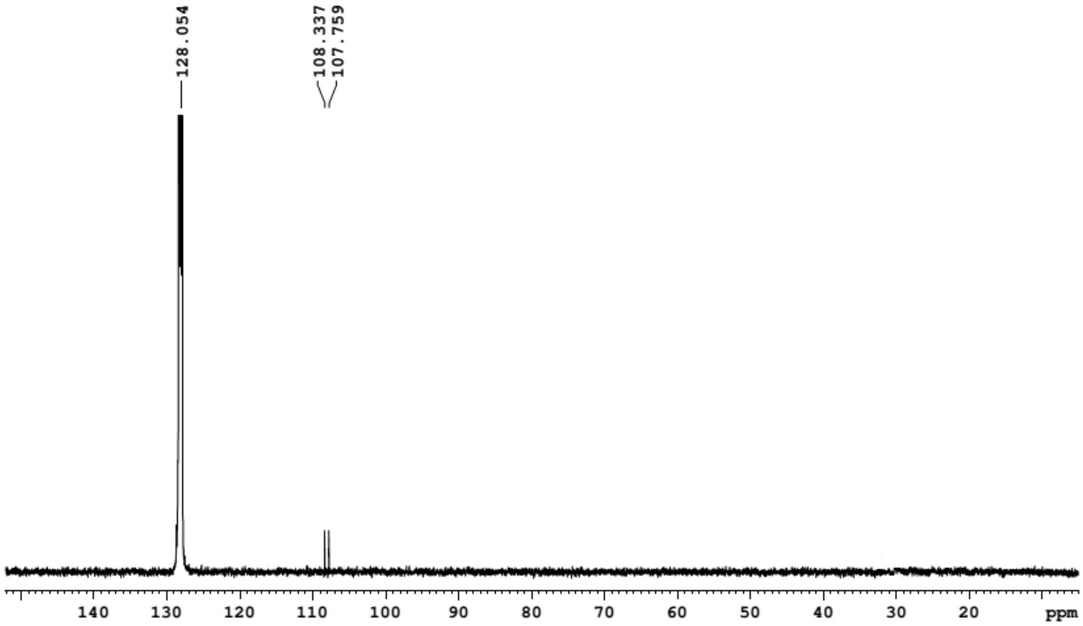

Fig. S19. $^{13}C\{^{1}H\}$ NMR spectrum of **2** in C_6D_6.

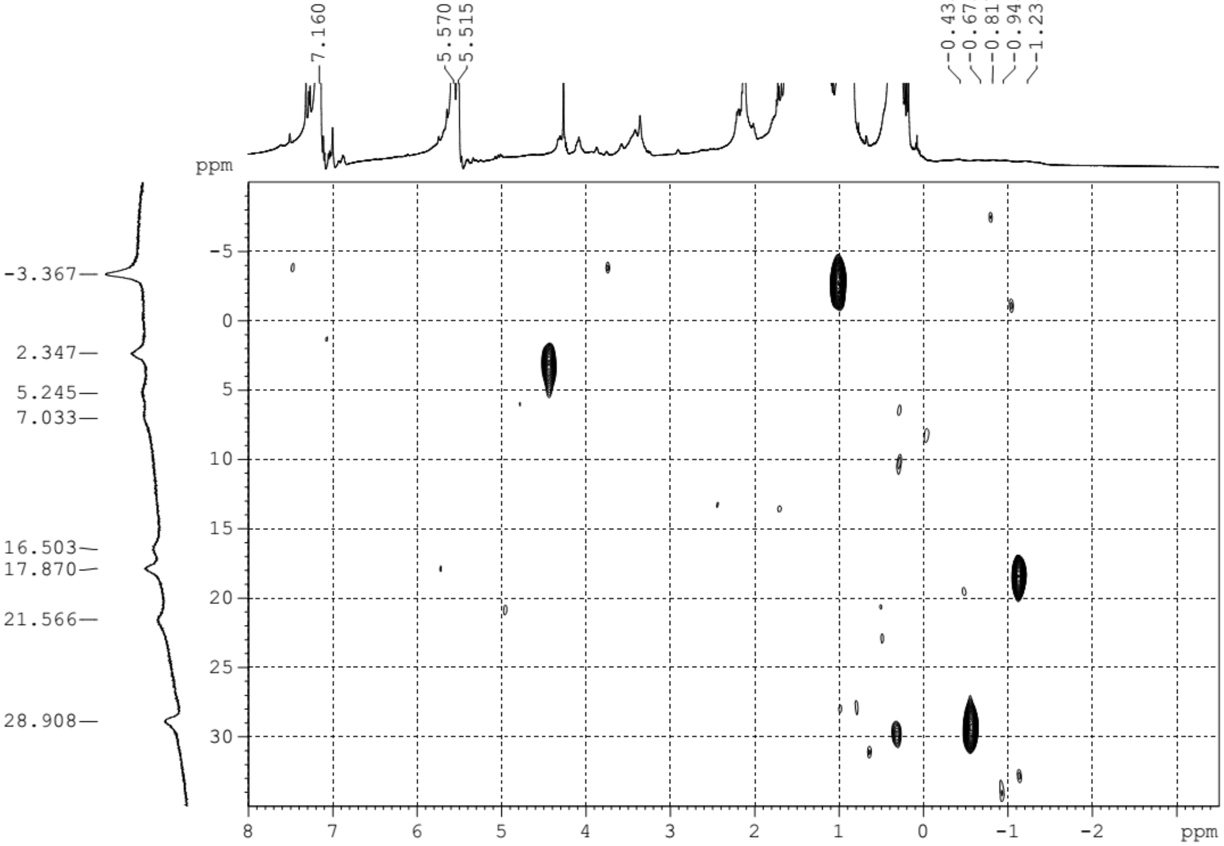

Fig. S20. $^{1}H\{^{11}B\}/^{11}B\{^{1}H\}$ HSQC spectrum of **2** in C_6D_6.

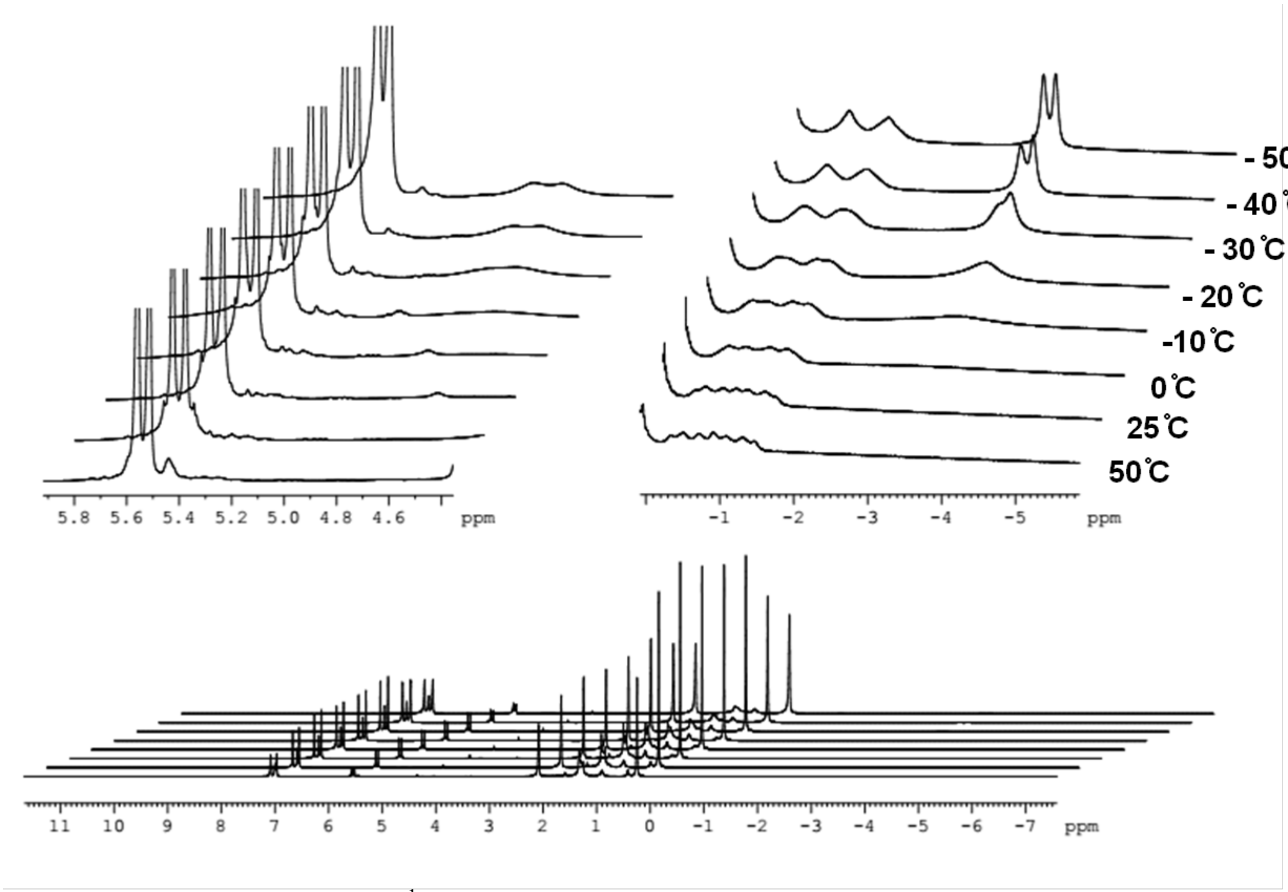

Fig. S21. Variable-temperature ^{1}H NMR spectra of **2** in [d_8]-toluene.

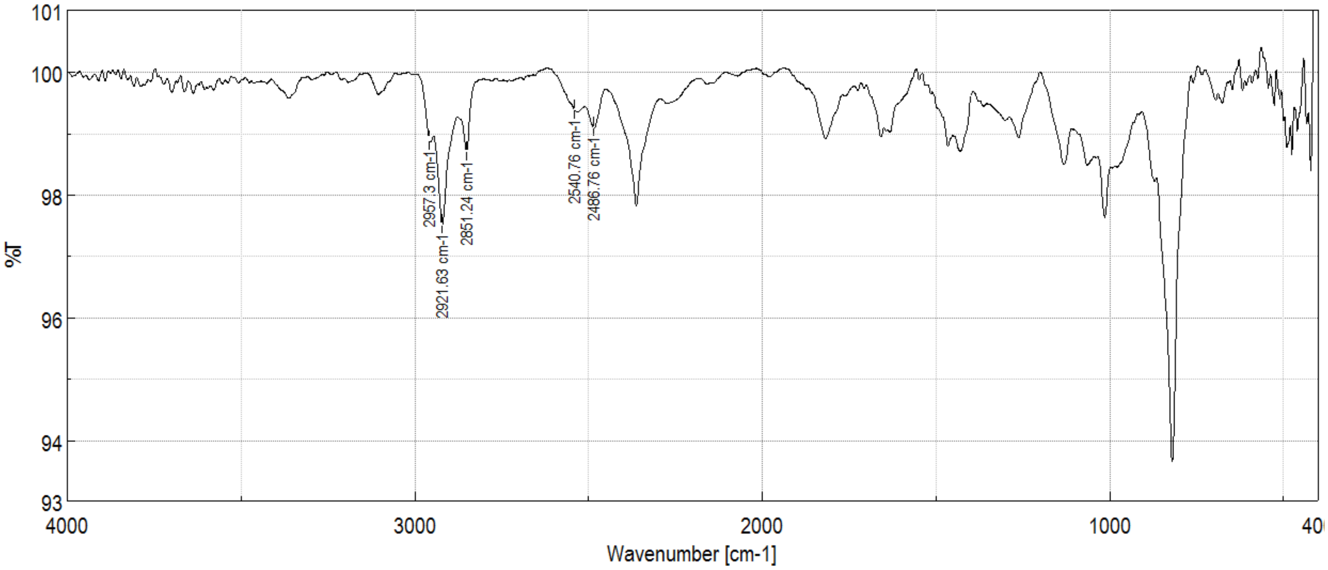

Fig. S22. IR spectrum of **2** in CH_2Cl_2.

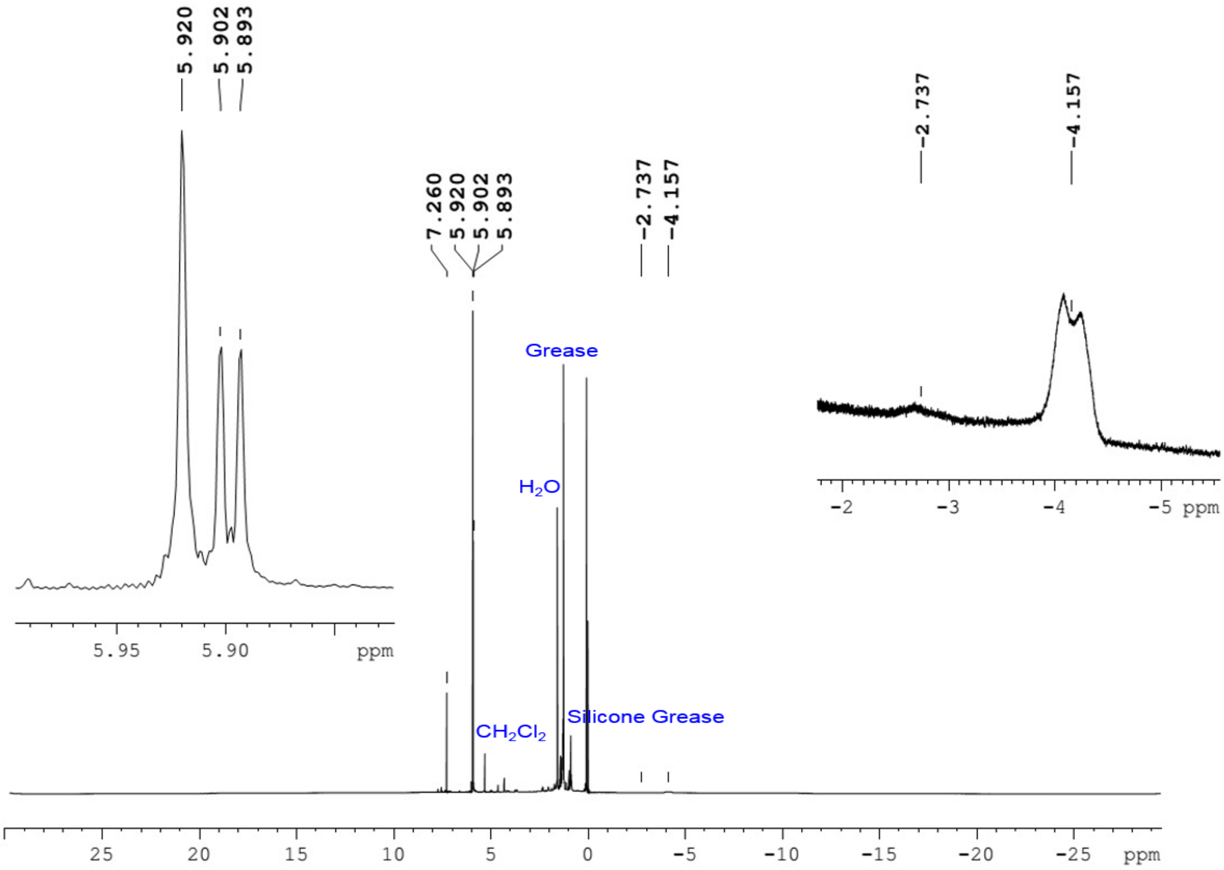

Fig. S23. ^{1}H NMR spectrum of **II** in CDCl$_3$.

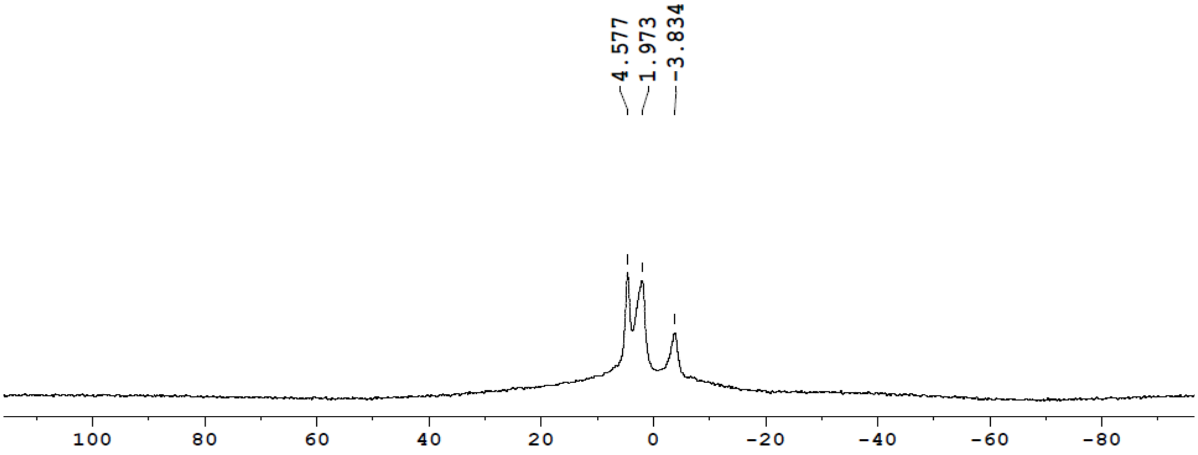

Fig. S24. ^{11}B{^{1}H} NMR spectrum of **II** in CDCl$_3$.

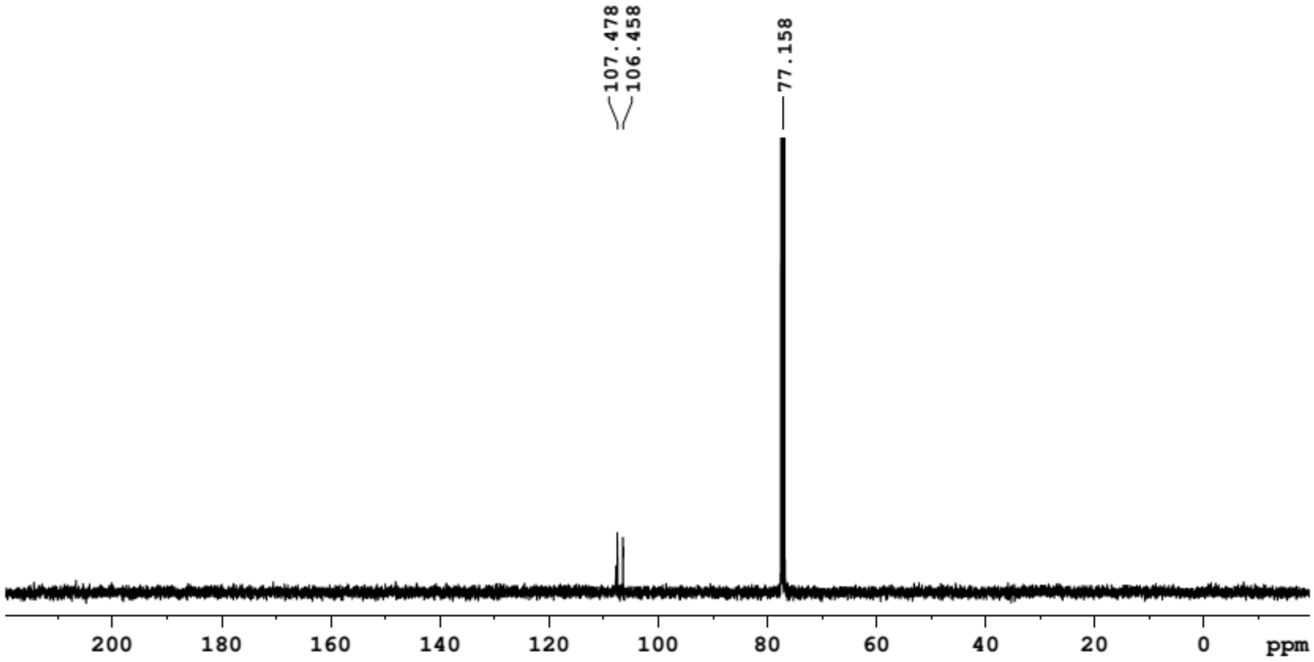

Fig. S25. $^{13}C\{^1H\}$ NMR spectrum of **II** in $CDCl_3$.

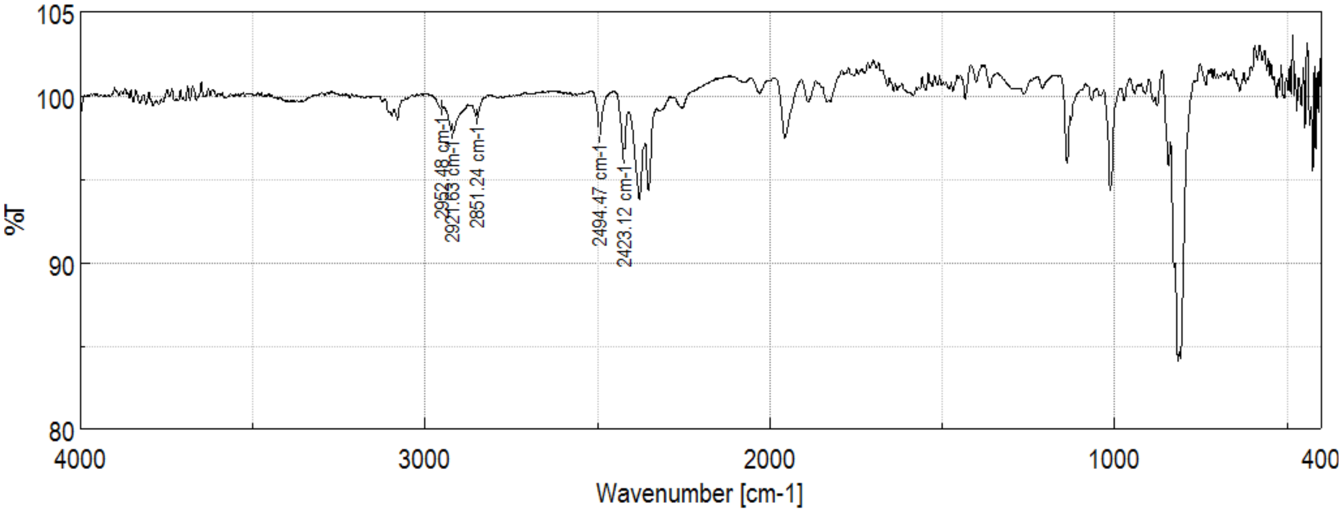

Fig. S26. IR spectrum of **II** in CH_2Cl_2.

IV X-ray Analysis Details

The crystal data for compounds **1** and **II** were collected and integrated using a Bruker AXS kappa APEX II CCD diffractometer, with graphite monochromated Mo Kα (λ = 0.71073 Å) radiation at 296 K (for **1**) and 293 K (for **II**), respectively. The crystal data for compounds **2** was collected and integrated using a Bruker apex3 C-MOS Diffractometer with micro focus Cu Kα (λ = 1.54178 Å) radiation at 293 K. The structures were solved by heavy atom methods using SHELXS-97 or SIR92[2] and refined using SHELXL-2014[3]. Crystallographic data have been deposited with the Cambridge Crystallographic Data Center as supplementary publication no. CCDC-1568097 (**1**), CCDC-1568096 (**2**) and CCDC-1568098 (**II**). These data can be obtained free of charge from The Cambridge Crystallographic Data Centre via www.ccdc.cam.ac.uk/data_request/cif

*Crystal data for **1***: $C_{27}H_{39}B_9Zr_2$, M_r = 643.31 g/mol, monoclinic, space group $P2_1/c$, a = 17.2544(6) Å, b = 12.8796(3) Å, c = 14.6295(5) Å, β = 109.855(2)°, V = 3057.85(17) Å^3, Z = 4, ρ_{calcd} = 1.397 g/cm^3, μ = 0.698 mm^{-1}, GOF = 1.021, $F(000)$ = 1304, R_1 = 0.0375, wR_2 = 0.0880, crystal size 0.35 × 0.22 × 0.10 mm^3, reflections collected 23741, independent reflections 5391 ($2\theta \leq 49.998°$) and 435 parameters.

*Crystal data for **2*** $C_{27}H_{35}B_9Hf_2$, M_r = 813.82 g/mol, monoclinic, space group $P2_1/c$, a = 17.2181(8) Å, b = 12.9003(7) Å, c = 14.6113(9) Å, β = 110.082(2)°, V = 3048.1(3) Å^3, Z = 4, ρ_{calcd} = 1.773 g/cm^3, μ = 12.444 mm^{-1}, GOF = 1.059, $F(000)$ = 1544, R_1 = 0.0783, wR_2 = 0.2342, crystal size 0.10 × 0.10 × 0.05 mm^3, reflections collected 50752, independent reflections 38138 ($2\theta \leq 64.983°$) and 360 parameters.

Crystal data for **II**: $C_{20}H_{24}B_5Hf_2$, M_r = 675.42 g/mol, monoclinic, space group Pc, a = 9.3061(8) Å, b = 7.8838(7) Å, c = 14.9171(12) Å, β = 100.720(2)°, V = 1075.33(16) Å^3, Z = 2, ρ_{calcd} = 2.086 g/cm^3, μ = 9.649 mm^{-1}, GOF = 1.022, $F(000)$ = 626, R_1 = 0.0396, wR_2 = 0.0968, crystal size 0.08 × 0.05 × 0.05 mm^3, reflections collected 18545, independent reflections 16245 ($2\theta \leq 56.0°$) and 259 parameters.

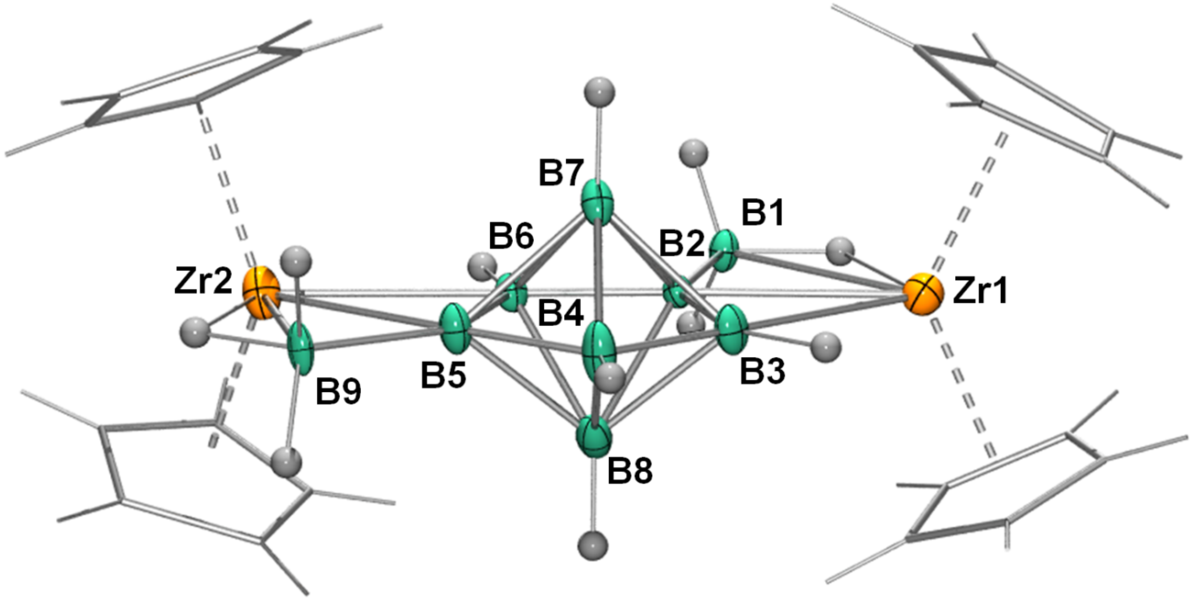

Fig. S27. Full molecular structure and labeling diagram for **1**. (Ellipsoids are set at 20% probablity, carbon and hydrogen atoms of Cp ring are not shown for clarity) Selected bond lengths (Å) and angles: B1-B2 1.761(5), B2-B3 1.606(5), B2-B6 1.656(6), B2-B7 1.879(6), B2-B8 1.880(6), B3-B4 1.648(6), B3-B7 1.788(7), B3-B8 1.788(7), B4-B5 1.647(6), B4-B7 1.775(8), B4-B8 1.784(8), B5-B6 1.615(6), B5-B7 1.844(7), B5-B8 1.855(7), B6-B7 1.794(6), B6-B8 1.798(6), B1-Zr1 2.561(4), B2-Zr1 2.437(4), B3-Zr1 2.479(4), B5-Zr2 2.453(4), B9-Zr2 2.550(5); B2-B1-Zr1 65.63(18), B2-B3-Zr1 69.5(2), B3-B2-B6 103.0(3), B3-B2-B1 145.6(3), B2-B3-B4 110.7(3), B3-B2-Zr1 72.4(2), B3-B4-B5 108.6(3), B6-B5-B4 103.6(3), B5-B6-B2 114.0(3), B4-B3-Zr1 179.6(4), B4-B5-Zr2 175.0(3), B6-B5-Zr2 71.5(2), B5-B6-Zr2 70.2(2).

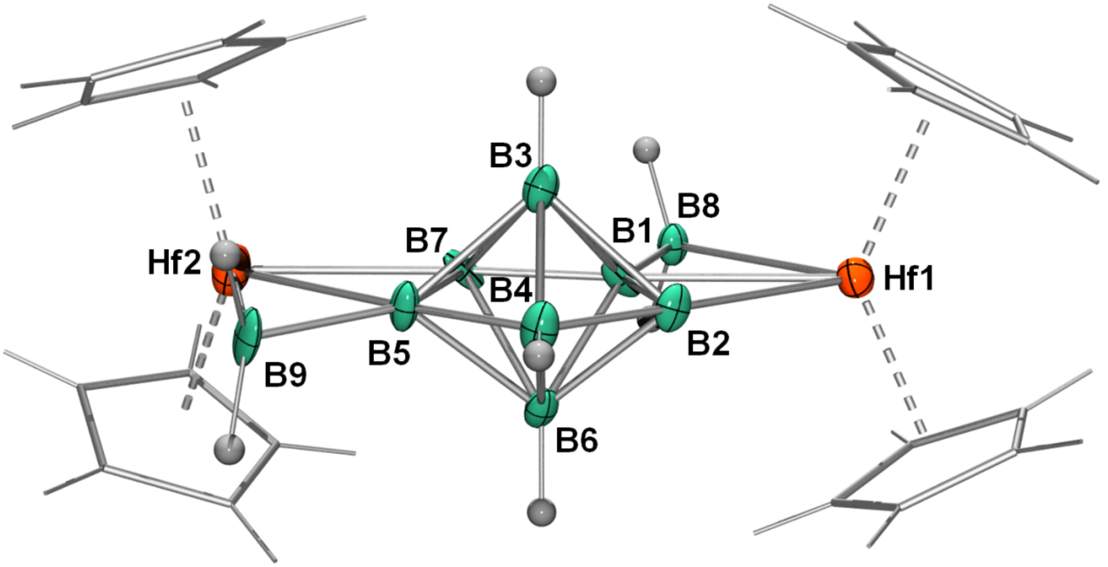

Fig. S28. Full molecular structure and labeling diagram of **2** (Some of the hydrogen atoms could not be located, ellipsoids are set at 20% probablity, carbon and hydrogen atoms of Cp ring are not shown for clarity). Selected bond lengths (Å) and angles (°): B1-B2 1.64(2), B1-B3 1.88(3), B1-B6 1.82(3), B1-B7 1.66(2), B1-B8 1.74(2), B2-B3 1.79(3), B2-B4 1.65(3), B2-B6 1.79(3), B3-B4 1.75(4), B3-B5 1.81(3), B3-B7 1.74(3), B4-B5 1.65(3), B4-B6 1.78(4), B5-B7 1.59(3), B5-B9 1.75(3), B5-B6 1.84(3), B6-B7 1 Hf2 2.49(3); B2-B1-B7 103.4(13), B2-B1-B8 143.5(13), B2-B1-Hf1 71.4(9), B7-B1-Hf1 173.9(11), B8-B1-Hf1 72.2(8), B1-B2-B4 109.0(15), B1-B2-B3 66.4(12), B4-B2-B3 61.1(14), B1-B2-B6 64.0(11), B1-B2-Hf1 69.5(9), B2-B4-B5 109.4(17), B4-B2-Hf1 178.5(14), B7-B5-B4 104.3(14), B7-B5-B9 142.1(17), B4-B5-B9 113.5(17), B7-B5-Hf2 71.0(9), B4-B5-Hf2 175.3(14), B9-B5-Hf2 71.2(12), B5-B7-B1 113.6(12), B5-B7-Hf2 70.7(9), B1-B7-Hf2 174.5(11), B1-B8-Hf1 66.7(7), B5-B9-Hf2 67.0(11), B1-Hf1-B2 39.1(6).81(2), B1-Hf1 2.428(15), B2-Hf1 2.46(2), B8-Hf1 2.517(17), B5-Hf2 2.42(2), B7-Hf2 2.428(15), B9-

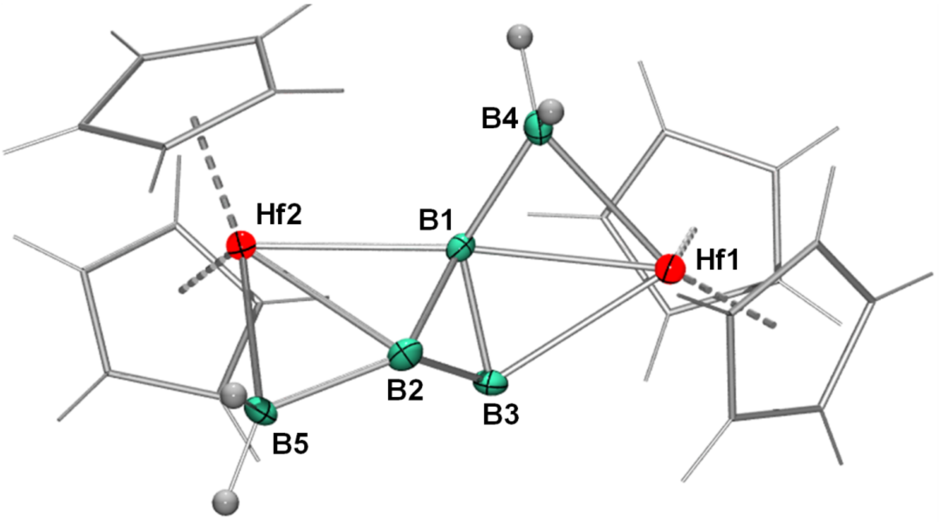

Fig. S29. Full molecular structure and labeling diagram of **II** (Some of the hydrogen atoms could not be located, ellipsoids are set at 20% probablity, carbon and hydrogen atoms of Cp ring are not shown for clarity). Selected bond lengths (Å) and angles (°): B1-B2 1.70(4), B1-B3 1.73(3), B1-B4 1.79(3), B1-Hf1 2.49(2), B1-Hf2 2.53(2), B2-B3 1.86(4), B2-B5 1.85(4), B2-Hf2 2.49(2), B3-Hf1 2.49(2); B2-B1-B3 65.6(15), B2-B1-B4 122.0(18), B3-B1-B4 137.8(18), B1-B3-B2 56.5(13), B2-B1-Hf1 112.6(15), B3-B1-Hf1 69.6(11), B4-B1-Hf1 69.9(11), B2-B1-Hf2 68.9(11), B4-B1-Hf2 119.4(14), Hf1-B1-Hf2 168.8(9), B1-B2-Hf2 71.4(12), B5-B2-Hf2 68.9(12), B1-B3-Hf1 69.7(10), B1-B4-Hf1 68.2(11).

VI Cluster valence electron (cve) count

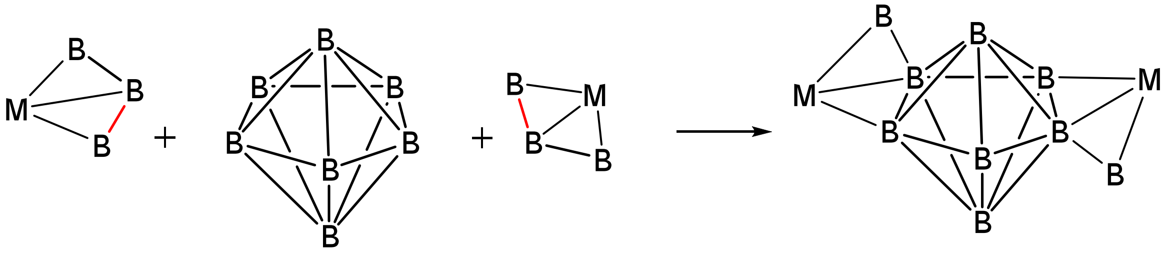

arachno-MB_3
(M = Zr or Hf)
(cve = 32)

closo-B_7
(cve = 30)

arachno-MB_3
(M = Zr or Hf)
(cve = 32)

1 or **2**
(M = Zr or Hf)
(cve = 66)

Scheme S1. Cluster valence electron (cve) count, for **1** or **2**. (*arachno*-MB_3 = [(14n+4n)+6]; *closo*-B_7 = [4n+2] and **1** or **2** = {2[(14n+4n)+6] + [4n+2] -2[6n+2]}.

Compound **1** or **2** can be considered as a fused cluster and according to Mingos fusion formalism the total cluster valence electron (cve) of such clusters is equal to the sum of the cve for the parent polyhedra minus the electron count of the shared unit (atom, pair of atoms, etc.). As shown in above Scheme S1, **1** or **2** can be described as fusion of two *arachno*-MB_3 (2{(14+12)+6} = 64e) and a *closo*-B_7 {(4×7+2) = 30} moieties through two B-B edges {2(6×2+2) = 28}. This arrangement of **1** or **2** generates electron count of 66e that is equal to its total cluster valence electron count (total cluster valence electrons of $[(Cp_2M)_2B_9H_{11}]$ = 2×14+9×3+11×1 = 66).

V Computational Details

All molecules were fully optimized with the Gaussian 09[4] program using the PBE1PBE(PBE0)[5] functional in conjunction with the def2-TZVP[6] basis set from EMSL[7] Basis Set Exchange Library. The 28 core electrons of zirconium and hafnium were replaced by the quasi-relativistic effective core potential def2-ECP.[8] The model compounds were fully optimized in gaseous state (no solvent effect) without any symmetry constraints. The crystallographic coordinates were used as a starting geometry for complete geometry optimizations. Frequency calculations were performed at the same level of theory to verify the nature of the stationary state and the absence of any imaginary frequency confirmed that all structures represent minima on the potential energy hypersurface. The binding energy calculation was carried out at the same level of theory. Further, gauge including atomic orbital (GIAO)[9-11] method has been employed to compute the ^{1}H and ^{11}B chemical shifts. The NMR chemical shifts were calculated using the hybrid Becke−Lee−Yang−Parr (B3LYP) functional [12] and def2-TZVP basis set on the PBE1PBE/def2-TZVP optimized geometries. The ^{11}B NMR chemical shifts were calculated relative to B_2H_6 (B3LYP B shielding constant 80.05 ppm) and converted to the usual [$BF_3.OEt_2$] scale using the experimental $\delta(^{11}B)$ value of B_2H_6, 16.6 ppm.[13] The aromaticity of the compounds was evaluated by calculating Nucleus Independent Chemical Shift (NICS)[14,15] indices on the optimized geometry at the same level of theory (PBE1PBE/def2-TZVP) by using the GIAO method implemented in Gaussian. As a normal routine, we placed ghost atoms at the ring critical point, the point of lowest density in the cage structure of each system,[16] to calculate the magnetic shielding tensor and measure aromaticity from the magnetic point of view. These values are denoted as NICS(0) as suggested by Schleyer et al.[14] Increasing aromaticity is indicated by more negative NICS values. It has been recommended to calculate NICS values at 1.0 Å above the perpendicular plane of the ring (NICS(1)) to get a better measure of π-aromaticity, as well as the $\mathrm{NICS(1)}_{ZZ}$ tensor component of this[17,18]. Adaptive natural density partitioning (AdNDP) method[19] was used for the bonding analysis of the opimized structures. The AdNDP analyses were carried out by utilizing Multiwfn V.3.3.8 package[20] whereas the wave functions were generated with Gaussian09 at the same level of theory as was used for geometry optimization. All the optimized structures and orbital graphics were generated using the GaussView[21], Jmol[22], VMD[23] and Molekel[24] visualization programs.

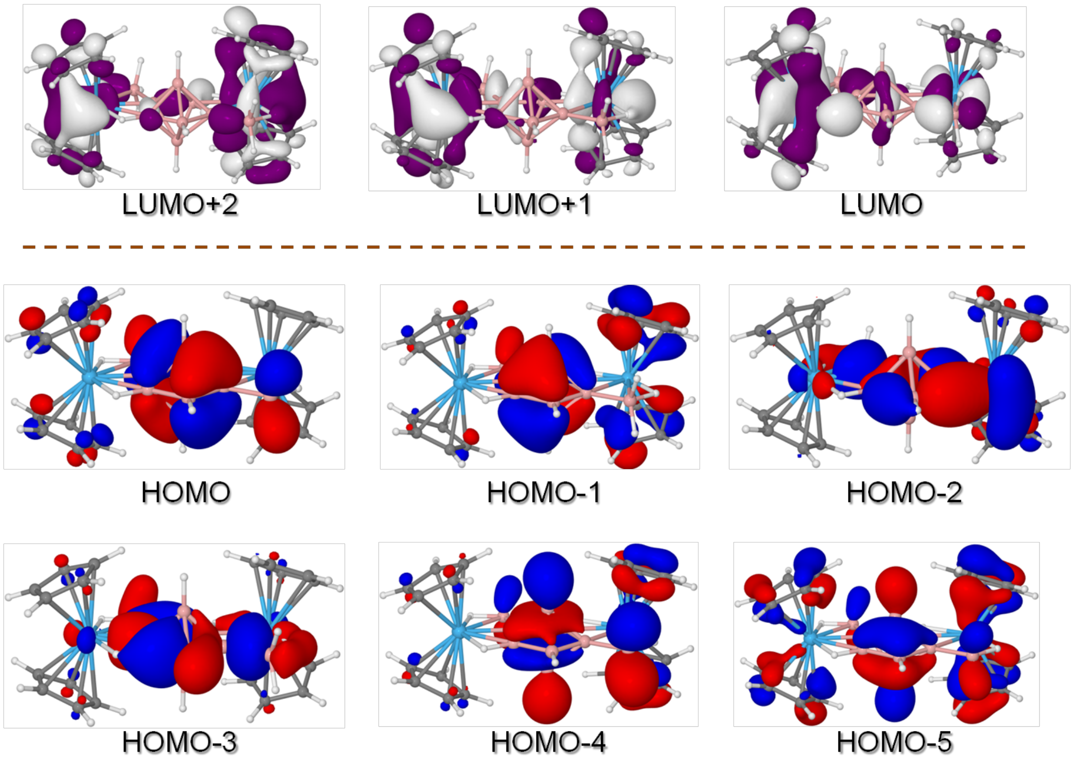

Fig. S30. Selected frontier molecular orbitals of **1** calculated at the PBE0/def2-TZVP level.

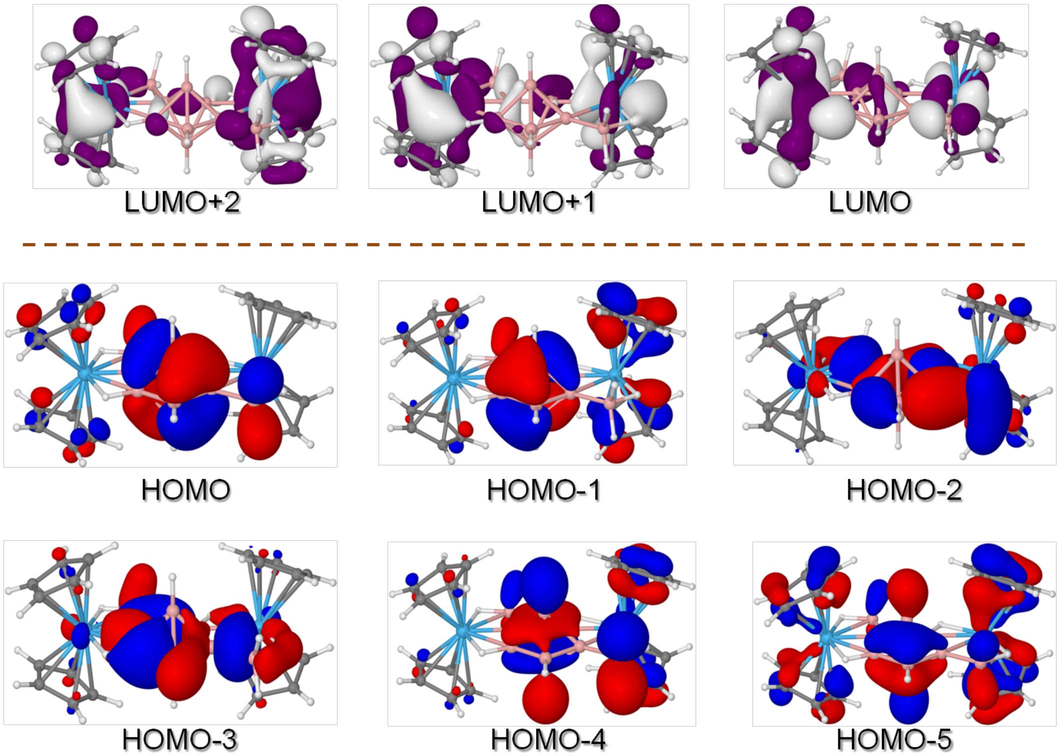

Fig. S31. Selected frontier molecular orbitals of **2** calculated at the PBE0/def2-TZVP level.

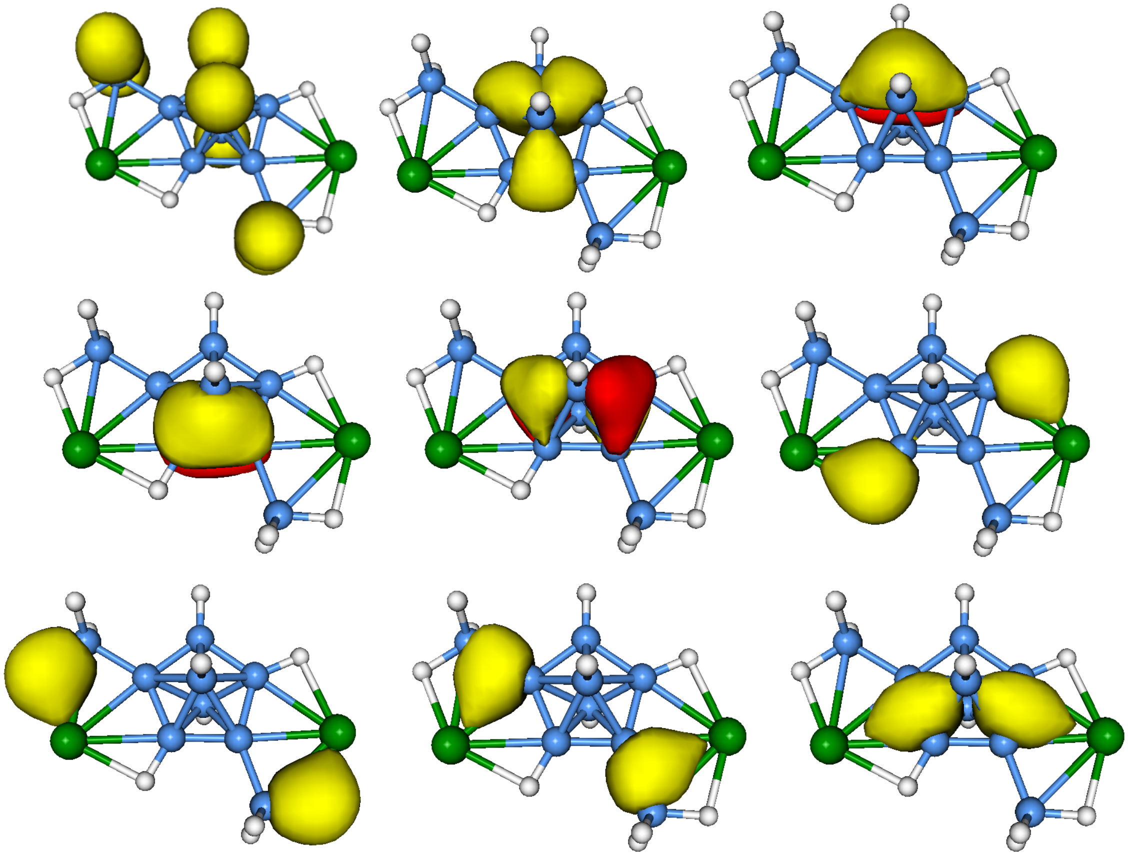

Fig. S32. AdNDP analysis of **1**.

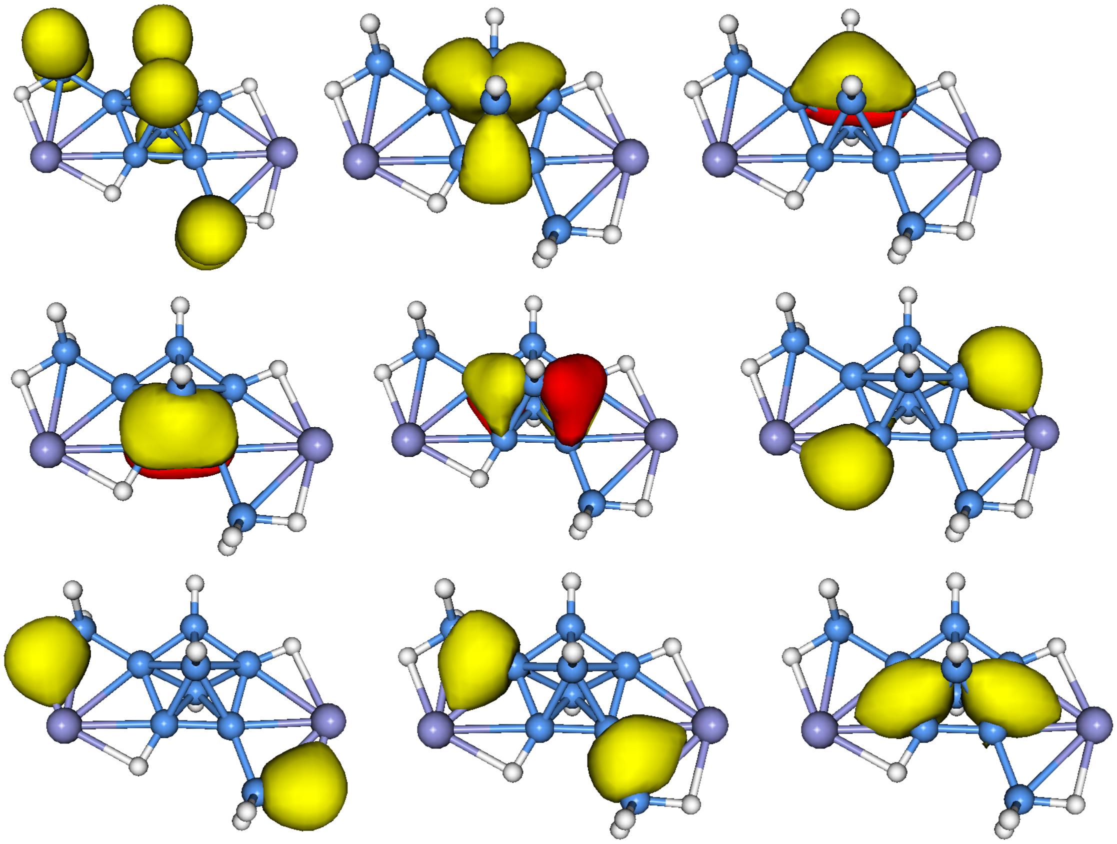

Fig. S33. AdNDP analysis of **2**.

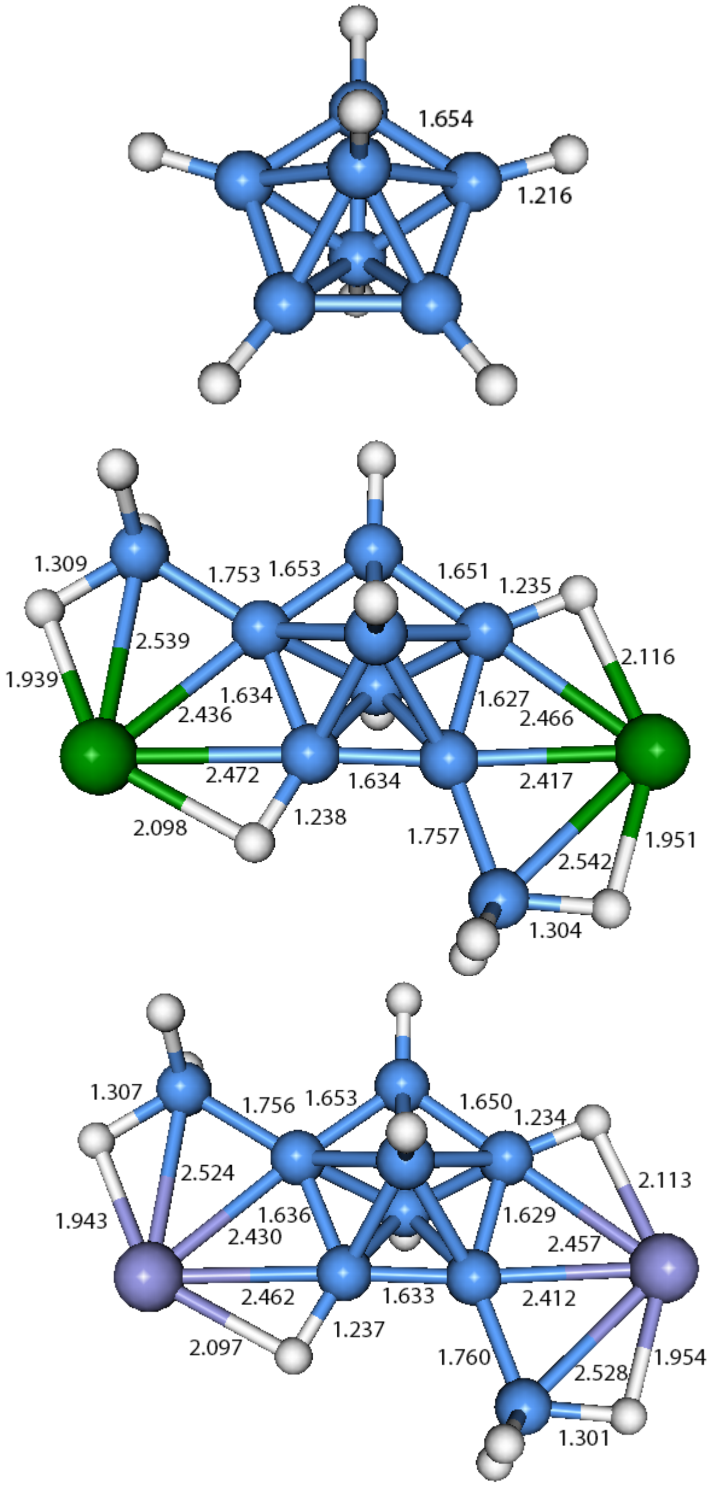

Fig. S34. Calculated bond lengths in Å for $[B_7H_7]^{2-}$, compound **1** and **2** (from top to bottom).

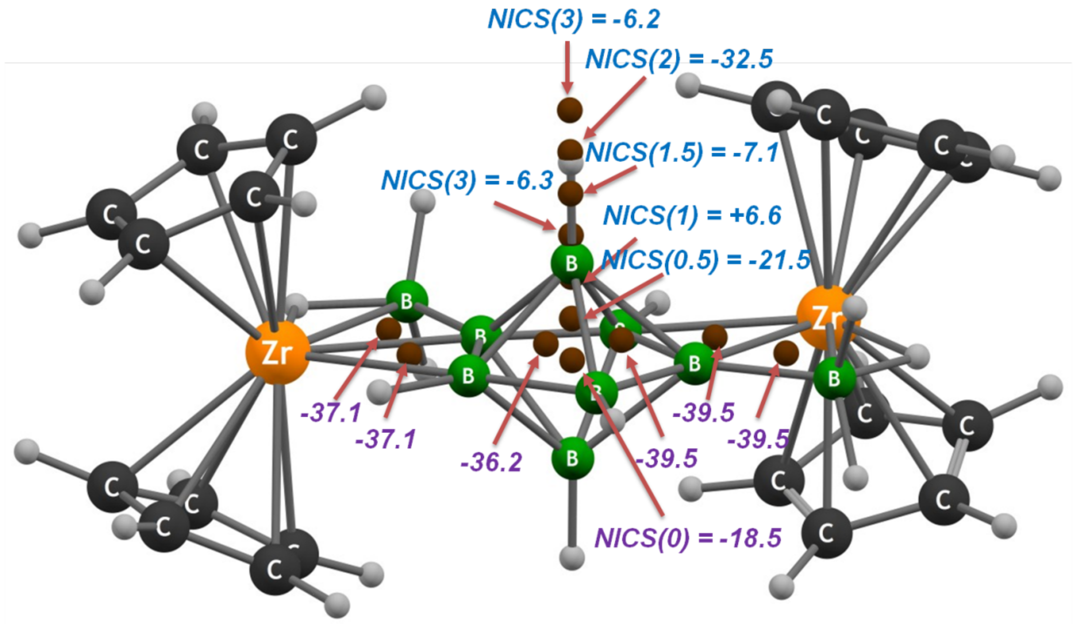

Fig. S35. Nucleus independent chemical shift (NICS) values of **1** calculated at GIAO-PBE1PBE/def2-TZVP level of theory.

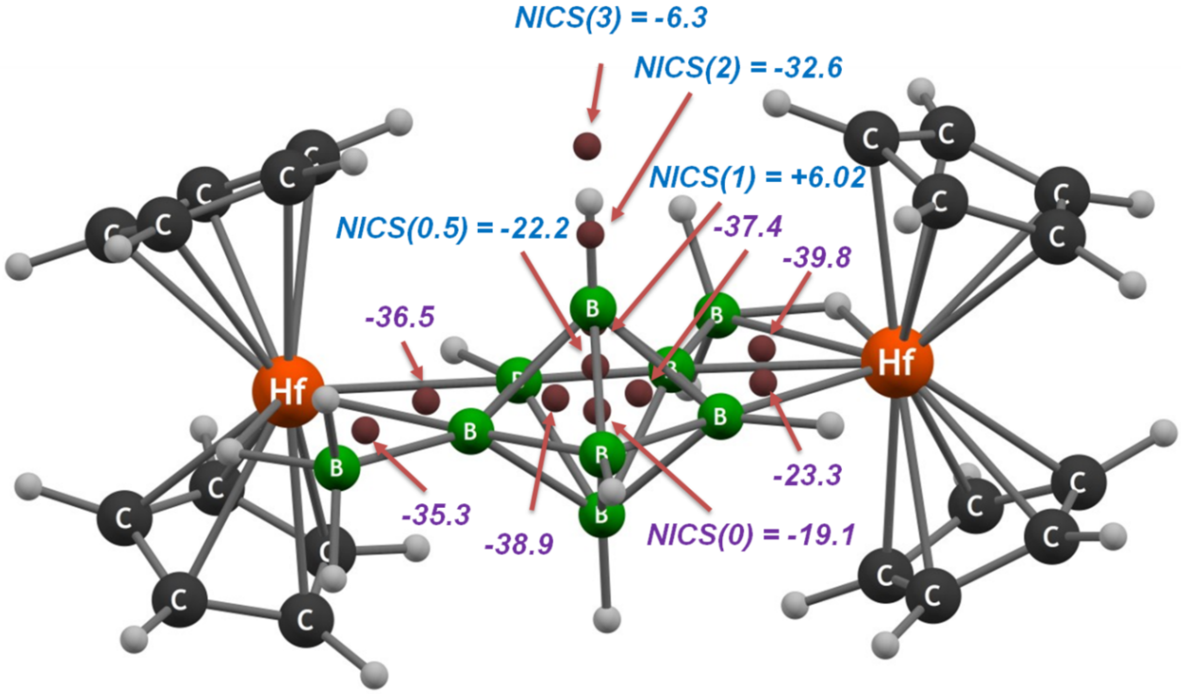

Fig. S36. Nucleus independent chemical shift (NICS) values of **2** calculated at GIAO-PBE1PBE/def2-TZVP level of theory.

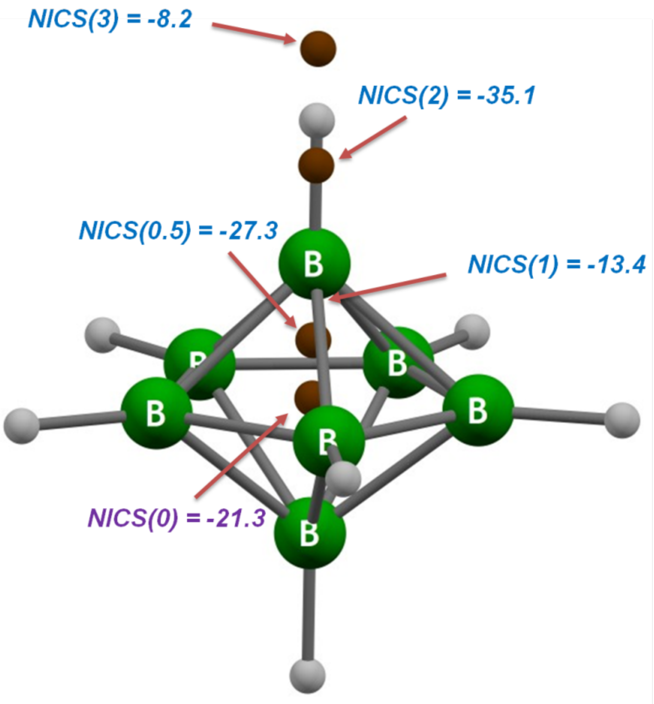

Fig. S37. Nucleus independent chemical shift (NICS) values of $[B_7H_7]^{2-}$ calculated at GIAO-PBE1PBE/def2-TZVP level of theory.

Table S1. Experimentally observed and calculated $^{11}B\{^{1}H\}$ chemical shifts of **1-2** and **I-II**.

	1		**2**		**II**		**I**	
	Expt.	*Cal.*	*Expt.*	*Cal.*	*Expt.*	*Cal.*	*Expt.*	*Cal.*
B1	6.3	10.1	16.2	14.5	4.6	1.5	-4.1	-1.4
B2	16.9	17.53	28.7	25.3	-3.8	-9.8	8.1	6.4
B3	29.1	30.47	-3.4	-5.62	-3.8	-5.8	2.5	-1.4
B4	0.8	0.05	2.4	0.35	4.6	2.3	8.1	9.1
B5	21.6	23.02	21.5	18.3	2.0	0.3	2.5	-4.5
B6	13.2	16.77	-3.4	-6.21			-	-
B7	-3.6	-5.2	17.8	15.8			-	-
B8	-3.6	-4.6	5.0	3.91			-	-
B9	6.8	10.9	6.5	3.94			-	-

References

1 G. E. Ryschkewitsch and K. C. Nainan, *Inorg. Synth*., 1974, **15**, 113.

2 G. M. Sheldrick, SHELXS-97, University of Göttingen, Germany, F.

3 G. M. Sheldrick, *Acta Crystallogr. Sect. C: Cryst. Struct. Commun.*, 2015, **71**, 3-8.

4 Gaussian 09, Revision C.01, M. J. Frisch, G. W. Trucks, H. B. Schlegel, G. E. Scuseria, M. A. Robb, J. R. Cheeseman, G. Scalmani, V. Barone, B. Mennucci, G. A. Petersson, H. Nakatsuji, M. Caricato, X. Li, H. P. Hratchian, A. F. Izmaylov, J. Bloino, G. Zheng, J. L. Sonnenberg, M. Hada, M. Ehara, K. Toyota, R. Fukuda, J. Hasegawa, M. Ishida, T. Nakajima, Y. Honda, O. Kitao, H. Nakai, T. Vreven, Jr. J. A. Montgomery, J. E. Peralta, F. Ogliaro, M. Bearpark, J. J. Heyd, E. Brothers, K. N. Kudin, V. N. Staroverov, T. Keith, R. Kobayashi, J. Normand, K. Raghavachari, A. Rendell, J. C. Burant, S. S. Iyengar, J. Tomasi, M. Cossi, N. Rega, J. M. Millam, M. Klene, J. E. Knox, J. B. Cross, V. Bakken, C. Adamo, J. Jaramillo, R. Gomperts, R. E. Stratmann, O. Yazyev, A. J. Austin, R. Cammi, C. Pomelli, J. W. Ochterski, R. L. Martin, K. Morokuma, V. G. Zakrzewski, G. A. Voth, P. Salvador, J. J. Dannenberg, S. Dapprich, A. D. Daniels, O. Farkas, J. B. Foresman, J. V. Ortiz, J. Cioslowski and D. J. Fox, Gaussian, Inc., Wallingford CT, **2010**.

5 J. P. Perdew, K. Burke and M. Ernzerhof, *Phys. Rev. Lett.*, 1996, **77**, 3865-3868.

6 F. Weigend and R. Ahlrichs, *Phys. Chem. Chem. Phys.*, 2005, **7**, 3297-3305.

7 EMSL Basis Set Exchange Library. https://bse.pnl.gov/bse/portal

8 D. Andrae, U. Häußermann, M. Dolg, H. Stoll and H. Preuss, *Theor. Chim. Acta.*, 1990, **77**, 123-141.

9 F. London, *J. Phys. Radium*., 1937, **8**, 397-409.

10 R. Ditchfield, *Mol. Phys.*, 1974, **27**, 789-807.

11 K. Wolinski, J. F. Hinton and P. Pulay, *J. Am. Chem. Soc.*, 1990, **112**, 8251-8260.

12 (a) A. D. Becke, *Phys. Rev. A.*, 1988, **38**, 3098-3100; (b) C. Lee, W. Yang and R. G. Parr, *Phys. Rev. B.*, 1988, **37**, 785-789; (c) A. D. Becke, *J. Chem. Phys.*, 1993, **98**, 5648-5652.

13 T. P. Onak, H. L. Landesman, R. E. Williams and I. Shapiro, *J. Phys.Chem.*, 1959, **63**, 1533-1535.

14 P. v. R. Schleyer, C. Maerker, A. Dransfeld, H. Jiao and N. J. R. v. E. Hommes, *J. Am. Chem. Soc.*, 1996, **118**, 6317-6318.

15 Z. Chen, C. S. Wannere, C. Cominboeuf, R. Puchta and P. v. R. Schleyer, *Chem. Rev.*, 2005, **105**, 3842-3888.

16 R. F. W. Bader, in *Atoms in Molecules: A Quantum Theory*, 2nd edn, Clarendon, Oxford, 1990.

17 P. v. R. Schleyer, M. Manoharan, H. J. Jiao and F. Stahl, *Org. Lett.*, 2001, **3**, 3643-3646.

18 C. Corminboeuf, T. Heine, G. Seifert, P. v. R. Schleyer and J. Weber, *Phys. Chem. Chem. Phys.*, 2004, **6**, 273-276.

19 D. Y. Zubarev and A. I. Boldyrev, *Phys. Chem. Chem. Phys.*, 2008, **10**, 5207–5217.

20 T. Lu and F. W. Chen, *J. Comput. Chem.*, 2012, **33**, 580–592.

21 GaussView, Version 3.09, Dennington II., R. T. Keith, J. Millam, K. Eppinnett, W. L. Hovell, R. Gilliland, Inc, Semichem, Shawnee Mission, KS, 2003.

22 Jmol: an open-source Java viewer for chemical structures in 3D. http://www.jmol.org/.

23 VMD-Visual Molecular Dynamics, W. Humphrey, A. Dalke, K. Schulten, *J. Molec. Graphics.*, 1996, **14**, 33-38. http://www.ks.uiuc.edu/Research/vmd/

24 U. Varetto, *Molekel 5.4*, Swiss National Supercomputing Center, Manno, Switzerland, 2009.